

THE DYNAMICS AND LIGHT CURVES OF BEAMED GAMMA RAY BURST AFTERGLOWS

JAMES E. RHOADS

Kitt Peak National Observatory, 950 North Cherry Avenue, Tucson, AZ 85719¹

Electronic mail: jrhoads@noao.edu

Submitted to *The Astrophysical Journal*, 2/1998; current revision 3/1999

ABSTRACT

The energy requirements of gamma ray bursts have in past been poorly constrained because of three major uncertainties: The distances to bursts, the degree of burst beaming, and the efficiency of gamma ray production. The first of these has been resolved, with both indirect evidence (the distribution of bursts in flux and position) and direct evidence (redshifted absorption features in the afterglow spectrum of GRB 970508) pointing to cosmological distances. We now wish to address the second uncertainty. Afterglows allow a statistical test of beaming, described in an earlier paper. In this paper, we modify a standard fireball afterglow model to explore the effects of beaming on burst remnant dynamics and afterglow emission. If the burst ejecta are beamed into angle ζ_m , the burst remnant's evolution changes qualitatively once its bulk Lorentz factor $\Gamma \lesssim 1/\zeta_m$: Before this, Γ declines as a power law of radius, while afterwards, it declines exponentially. This change results in a broken power law light curve whose late-time decay is faster than expected for a purely spherical geometry. These predictions disagree with afterglow observations of GRB 970508. We explored several variations on our model, but none seems able to change this result. We therefore suggest that this burst is unlikely to have been highly beamed, and that its energy requirements were near those of isotropic models. More recent afterglows may offer the first practical applications for our beamed models.

1. INTRODUCTION

Understanding the energy requirements and event rates of gamma ray bursts is necessary for any quantitative evaluation of a candidate burst progenitor. We need to know both how many progenitors we expect, and how much energy they need to produce in a single event. Until recently, both quantities were uncertain to ~ 10 orders of magnitude because of the unknown distance to the bursts. The afterglow of GRB 970508 effectively ended that debate, because it showed absorption lines at a cosmological redshift ($z = 0.835$; Metzger et al 1997). This builds on earlier results from the Burst and Transient Source Experiment (BATSE), which showed that the burst distribution on the sky is exquisitely isotropic while the distribution in flux is inhomogeneous (Meegan et al 1996). These observations are best explained if the bursts are at cosmological distances. A very extended Galactic halo distribution might also work, but it would have to be unlike any other known population of Galactic objects. The isotropy is perhaps most important now for showing that multiple-population scenarios for gamma ray bursts cannot put any substantial fraction of the bursters at Galactic distances. It thus connects the GRB 970508 redshift bound to the vast majority of the burst population.

The dominant remaining uncertainty in the bursters' energy requirements is now whether the bursts radiate isotropically or are beamed into a very small solid angle. Such beaming is allowed (though not required) by the gamma ray observations, because the ejecta from gamma ray bursts must be highly relativistic to explain the spectral properties of the emergent radiation (Paczynski 1986,

Goodman 1986), with inferred minimum Lorentz factors $\Gamma \gtrsim 100$ (Woods & Loeb 1995). The gamma rays we observe are therefore only those from material moving within angle $1/\Gamma$ of the line of sight, and offer no straightforward way of determining whether there are ejecta outside this narrow cone.

These large Lorentz factors lead naturally to predictions of afterglow emission at longer wavelengths as the burst ejecta decelerate and interact with the surrounding material (Paczynski & Rhoads 1993; Katz 1994; Mészáros & Rees 1997a). The characteristic frequency for this afterglow emission depends on the Lorentz factor of the burst remnant, and both decrease as the remnant evolves. Such models scored a recent triumph with the detection of X-ray, optical, and radio afterglows from gamma ray bursts (GRBs) early in 1997 (e.g., Costa et al 1997; van Paradijs et al 1997; Bond 1997; Frail et al 1997). The observed properties of the transients are in good overall agreement with the predictions of afterglow models (Wijers, Rees, & Mészáros 1997; Waxman 1997a,b), although some worries remain (Dar 1997).

Because beaming depends on the relativistic nature of the flow, afterglows can be used to test the burst beaming hypothesis. At least two such tests are possible. First, because Γ is lower at the time of afterglow emission than during the GRB itself, the afterglow cannot be as collimated as the GRB can. This implies that the afterglow event rate should exceed the GRB event rate substantially if bursts are strongly beamed. Allowing for finite detection

¹Postal address: P.O. Box 26732, Tucson, AZ 85726-6732

thresholds,

$$\frac{N_{12}}{N_2} \leq \frac{\Omega_1}{\Omega_2} \leq \frac{N_1}{N_{12}} \quad , \quad (1)$$

where N_1 , N_2 are the measured event rates above our detection thresholds at our two frequencies; N_{12} is the rate of events above threshold at both frequencies; and Ω_1 , Ω_2 are the solid angles into which emission is beamed at the two frequencies. A full derivation of this result and discussion of its application is given in Rhoads (1997a).

The second test is based on differences between the dynamical evolution of beamed and isotropic bursts. Burst ejecta decelerate through their interaction with the ambient medium. If the ejecta are initially beamed into a cone of opening angle ζ_m , the deceleration changes qualitatively when the bulk Lorentz factor Γ drops to $1/\zeta_m$. Prior to this, the working surface (i.e. the area over which the expanding blast wave interacts with the surrounding medium) scales as r^2 . At later times, the ejecta cloud has undergone significant lateral expansion in its frame, and the working surface increases more rapidly with r , eventually approaching an exponential growth. Spherical symmetry prevents this transition from occurring in unbeamed bursts. A brief analysis of this effect was presented in Rhoads (1997b).

We have two major aims in this paper. First, we will present a full derivation of the late time burst remnant dynamics for a beamed gamma ray burst. We support this by calculating the emergent synchrotron radiation for two electron energy distribution models, but we do not attempt to do so for all possible fireball emission scenarios. Second, we observe that our model is not consistent with any small-angle beaming of GRB 970508. This implies a substantial minimum energy for this burst. If radiative efficiencies are lower than $\sim 10\%$, this limit approaches the maximum energy available in compact object merger events. We explore possible ways to evade this minimum energy requirement through other forms of beaming models, but find none. We therefore conjecture that such models cannot be constructed for GRB 970508 unless the usual fireball model assumptions about relativistic blast wave physics are substantially modified, and challenge the community to prove this assertion right or wrong.

We explore the dynamical evolution of a model beamed burst in section 2. In section 3 we incorporate a model for the electron energy spectrum and magnetic field strength and so predict the emergent synchrotron radiation. In section 4, we compare the model with observed afterglows. The early (1997) data appeared inconsistent with the beaming model, suggesting that bursts are fairly isotropic and therefore very energetic events. Finally, in section 4.1, we explore variations on our model to try to reduce the inferred energy needs of GRB 970508. We comment briefly on more recent data and summarize our conclusions in section 5.

2. DYNAMICAL CONSEQUENCES OF BEAMING

We explore the effects of beaming on burst evolution using the notation of Paczyński & Rhoads (1993). Let Γ_0 and M_0 be the initial Lorentz factor and ejecta mass, and ζ_m the opening angle into which the ejecta move. The burst energy is $E_0 = \Gamma_0 M_0 c^2$. Let r be the radial coordinate in the burster frame; t , t_{co} , and t_{\oplus} the time from

the event measured in the burster frame, comoving ejecta frame, and terrestrial observer's frame; and f the ratio of swept up mass to M_0 .

The key assumptions in our beamed burst model are that (1) the initial energy and mass per unit solid angle are constant at angles $\theta < \zeta_m$ from the jet axis and zero for $\theta > \zeta_m$; (2) the total energy in the ejecta + swept-up material is approximately conserved; (3) the ambient medium has uniform density ρ ; and (4) the cloud of ejecta + swept-up material expands in its comoving frame at the sound speed $c_s = c/\sqrt{3}$ appropriate for relativistic matter. The last of these assumptions implies that the working surface of the expanding remnant has a transverse size $\sim \zeta_m r + c_s t_{co}$. The evolution of the burst changes when the second term dominates over the first.

Each of these assumptions may be varied, but we believe the qualitative change in burst remnant evolution will remain over a wide range of possible beaming models. Removing assumption (4) is the only obvious way to turn off the dynamical effects of beaming, and even then observable breaks in the light curve are expected when $\Gamma \sim 1/\zeta_m$.

There are several models in the literature that use radiative rather than adiabatic models, dropping our second assumption. The case for radiative bursts depends on the efficiency with which relativistic shocks transfer bulk kinetic energy to magnetic fields and electrons, and I regard the validity of assumption (2) as an open question. For a closer examination of this issue, I refer the reader to papers by Vietri (1997a,b) and by Katz & Piran (1997a), who advocate radiative models; and to Waxman, Kulkarni, & Frail (1998), who defend the adiabatic model. Mészáros, Rees, & Wijers (1997) point out that the dynamical consequences ($\Gamma \propto r^{-3}$) of radiative models depend on equipartition between protons, electrons, and magnetic fields being maintained at all times. Thus, a short electron cooling time will affect the afterglow radiation, but will not necessarily result in $\Gamma \propto r^{-3}$. Sari (1997) considers corrections to the adiabatic burst evolution for modest energy losses.

Models that do not use assumption (1) have been discussed by Mészáros, Rees, & Wijers (1997) and Panaitescu, Mészáros, & Rees (1998). Finally, assumption (3) has been dropped by several authors (Vietri 1997b; Mészáros, Rees, & Wijers 1997; Panaitescu, Mészáros, & Rees 1998) in favor of a more general power law density $\rho \propto r^{-g}$. Such models complicate the beamed burst analysis and will change the form of $\Gamma(r)$ relation but will leave intact the basic conclusion that $\Gamma(r)$ changes qualitatively when $\Gamma \lesssim 1/\zeta_m$.

2.1. Dynamical Calculations: Numerical Integrations

Given these assumptions, the full equations describing the burst remnant's evolution are

$$f = \frac{1}{M_0} \int_0^r r^2 \Omega_m(r) \rho(r) dr \quad , \quad (2)$$

$$\Omega_m \approx \pi(\zeta_m + c_s t_{co}/ct)^2 \approx \pi(\zeta_m + t_{co}/\sqrt{3}t)^2 \quad , \quad (3)$$

$$\Gamma = (\Gamma_0 + f) / \sqrt{1 + 2\Gamma_0 f + f^2} \approx \sqrt{\Gamma_0/2f} \quad , \quad (4)$$

$$t = r/c \quad , \quad t_{co} = \int_0^t dt' / \Gamma \quad ,$$

$$\text{and } t_{\oplus} = (1+z) \int_0^t dt'/2\Gamma^2. \quad (5)$$

Equation 4 is derived in Paczyński & Rhoads (1993) from conservation of energy and momentum, along with algebraic simplifications of equations 5 for the spherical case. The definition of t_{\oplus} here includes the cosmological time dilation factor $(1+z)$ for a source at redshift z . Equation 3 is not strictly valid when $\zeta_m \gtrsim 1$, but we will accept this deficiency since the error thereby introduced is not a dominant uncertainty in our results.

These equations can be solved by numerical integration to yield $f(r)$, $\Gamma(r)$, and $t_{\oplus}(r)$. Figure 1 shows $\Gamma(r)$ from such integrations for an illustrative pair of models (one beamed, one isotropic).

2.2. Dynamical Calculations: Analytic Integrations

The most interesting dynamical change introduced by beaming is a transition from a power law $\Gamma \propto r^{-3/2}$ to an exponentially decaying regime $\Gamma \propto \exp(-r/r_{\Gamma})$. We will first give a derivation of the power law behavior.

2.2.1. Power Law Regime

Consider the approximate evolution equations for the regime where (a) $1/\Gamma_0 \lesssim f \lesssim \Gamma_0$, so that $\Gamma \approx \sqrt{\Gamma_0/2f}$; and (b) $c_s t_{co} \lesssim \zeta_m r$ (corresponding to $f \lesssim 9\Gamma_0 \zeta_m^2$).

$$\begin{aligned} df/dr &\approx \frac{\pi}{M_0} (\zeta_m r)^2 \rho, & dt_{co}/dr &\approx \sqrt{\frac{2f}{c^2 \Gamma_0}}, \\ dt_{\oplus}/dr &\approx (1+z) \frac{f}{c\Gamma_0}. \end{aligned} \quad (6)$$

The initial conditions are $f = 0$ and $t = t_{co} = t_{\oplus} = 0$ at $r = 0$. So we can easily integrate and obtain

$$f = \frac{\pi \zeta_m^2 \rho}{3 M_0} r^3, \quad (7)$$

$$\Gamma \approx \left(\frac{3M_0 \Gamma_0}{2\pi \zeta_m^2 r^3 \rho} \right)^{1/2} = \left(\frac{3E_0}{2\pi \zeta_m^2 c^2 r^3 \rho} \right)^{1/2} \quad (8)$$

$$t_{co} = \left(\frac{8\pi \zeta_m^2 \rho}{75 E_0} \right)^{1/2} r^{5/2} = \frac{2}{5} \frac{r}{c\Gamma} \quad (9)$$

$$t_{\oplus} = (1+z) \frac{\pi \zeta_m^2 c \rho}{12 E_0} r^4 \quad (10)$$

whence

$$\Gamma = 2^{-5/4} \left(\frac{3E_0}{\pi \zeta_m^2 c^2 \rho} \right)^{1/8} \left(\frac{1+z}{ct_{\oplus}} \right)^{3/8}. \quad (11)$$

By making the substitutions $\pi \zeta_m^2 \rightarrow 4\pi$ and $(1+z) \rightarrow 1$ in these results, we recover the evolution of a spherically symmetric burst remnant derived by Paczyński & Rhoads (1993).

2.2.2. Exponential Regime

To demonstrate the exponential behavior, consider the approximate evolution equations for the regime where (a) $1/\Gamma_0 \lesssim f \lesssim \Gamma_0$, so that $\Gamma \approx \sqrt{\Gamma_0/2f}$; and (b) $c_s t_{co} > \zeta_m r$ (corresponding to $f \gtrsim 9\Gamma_0 \zeta_m^2$):

$$\begin{aligned} df/dr &\approx \frac{\pi}{M_0} c_s^2 t_{co}^2 \rho, & dt_{co}/dr &\approx \sqrt{\frac{2f}{c^2 \Gamma_0}}, \\ dt_{\oplus}/dr &\approx (1+z) \frac{f}{c\Gamma_0}. \end{aligned} \quad (12)$$

By forming the ratio $(df/dr)/(dt_{co}/dr)$ and isolating terms with f and with t_{co} , it follows that

$$\sqrt{f} df = \frac{\pi}{\sqrt{2}} \frac{c c_s^2 \rho \sqrt{\Gamma_0}}{M_0} \times t_{co}^2 dt_{co} \approx \frac{\pi}{3\sqrt{2}} \frac{c^3 \rho \sqrt{\Gamma_0}}{M_0} \times t_{co}^2 dt_{co}. \quad (13)$$

This is easily integrated to obtain

$$f^{3/2} = \left(\frac{\pi \sqrt{\Gamma_0} c c_s^2 \rho}{\sqrt{8} M_0} \right) (t_{co}^3 - c_1), \quad (14)$$

where c_1 is a constant of integration. Using the initial conditions for the exponential regime derived below (eqn. 16 – 19), one can show that the constant of integration is $c_1 = -25E_0 \zeta_m^3 / (4\pi \rho c_s^5)$, which becomes negligible once $c_s t_{co} \gg \zeta_m r$. Equation 14 then becomes $f \propto t_{co}^2$, and we see from equations 12 and 4 that f , Γ , t_{co} , and t_{\oplus} will all behave exponentially with r in this regime. Retaining the constants of proportionality, we find

$$\begin{aligned} f &\propto \exp(2r/r_{\Gamma}) \quad \text{where} \\ r_{\Gamma} &= \left[\frac{1}{\pi} \left(\frac{c}{c_s} \right)^2 \frac{\Gamma_0 M_0}{\rho} \right]^{1/3} = \left[\frac{E_0}{\pi c_s^2 \rho} \right]^{1/3}. \end{aligned} \quad (15)$$

Further algebra yields $\Gamma \propto \exp(-r/r_{\Gamma})$, $t_{co} \propto \sqrt{f} \propto \exp(r/r_{\Gamma})$, and $t_{\oplus} \propto f \propto \exp(2r/r_{\Gamma})$, so that $\Gamma \propto t_{\oplus}^{-1/2}$. Thus, while the evolution of $\Gamma(r)$ changes from a power law to an exponential at $\Gamma \sim 1/\zeta_m$, the evolution of $t_{\oplus}(r)$ changes similarly. The net result is that $\Gamma(t_{\oplus})$ has a power law form in both regimes, but with a break in the slope from $\Gamma \propto t_{\oplus}^{-3/8}$ when $\Gamma > 1/\zeta_m$ to $\Gamma \propto t_{\oplus}^{-1/2}$ when $\Gamma < 1/\zeta_m$.

The initial conditions for the exponential regime are approximately set by inserting the transition condition $c_s t_{co} = \zeta_m r$ into the evolution equations for the power law regime. Denoting the values at this break with the subscript b , we have $c_s t_{co,b} = \zeta_m r_b = \zeta_m t_b$, which we combine with equation 9 to obtain

$$r_b = \left(\frac{75 E_0}{8\pi \rho c_s^2} \right)^{1/3} \quad \text{and} \quad f_b = \frac{25}{8} \left(\frac{c}{c_s} \right)^2 \zeta_m^2 \Gamma_0. \quad (16)$$

The corresponding values for Γ , t_{\oplus} , and t_{co} are

$$\Gamma_b = \frac{2c_s}{5c} \frac{1}{\zeta_m}, \quad (17)$$

$$t_{\oplus,b} = (1+z) \left(\frac{3}{\pi} \right)^{1/3} \frac{5^{8/3}}{64} \frac{c}{c_s} \left(\frac{E_0}{\rho c_s^5} \right)^{1/3} \zeta_m^2 \quad (18)$$

$$\text{and } t_{co,b} = \zeta_m \left(\frac{75 E_0}{8\pi \rho c_s^5} \right)^{1/3} \quad (19)$$

The evolution in the exponential regime is then approximated by

$$\begin{aligned} f &= f_b \times \exp\{2(r-r_b)/r_\Gamma\} \\ t_\oplus &= t_{\oplus,b} \times \exp\{2(r-r_b)/r_\Gamma\} \\ \Gamma &= \Gamma_b \times \exp\{-(r-r_b)/r_\Gamma\} \\ t_{co} &= t_{co,b} \times \exp\{(r-r_b)/r_\Gamma\} \end{aligned} \quad (20)$$

A thought experiment that will help understand the onset of the exponential decay of Γ with radius is to consider the shape of a GRB remnant in a pressureless, uniform ambient medium at late times (after all motions have become nonrelativistic). In the spherical case, the blast wave will leave behind a spherical cavity. In the beamed geometry, the cavity will be conical near the burster, but will change shape at the radius where the lateral expansion of the remnant becomes important. At this point, the cone flares, and the mass swept up per unit distance begins to grow faster than r^2 . This corresponds to the onset of the exponential $\Gamma(r)$ regime. The cone continues to become rapidly wider until it reaches the radius where the remnant becomes nonrelativistic. The final cavity resembles the bell of a trumpet. It is unclear whether such remnants would survive long enough to be observed in a realistic interstellar medium.

3. EMERGENT RADIATION

The Lorentz factor Γ is not directly observable, and we ultimately want to predict observables like the frequency of peak emission $\nu_{\oplus,m}$, the flux density $F_{\nu_{\oplus,m}}$ at $\nu_{\oplus,m}$, and the angular size θ of the afterglow. To do so, we need to introduce a model for the emission mechanism. We will restrict our attention to synchrotron emission, which is the leading candidate for GRB afterglow emission. We first consider the case of optically thin emission with a steep electron energy spectrum. This emission model is used in many recent afterglow models (e.g. Waxman 1997a,b). We then repeat the calculation for the emission model of Paczyński & Rhoads (1993).

3.1. General equations: Optically thin case

Our dynamical model for burst remnant evolution gives the volume V and internal energy density u_i of the ejecta as a function of expansion radius r . Detailed predictions of synchrotron emission require the magnetic field strength and the electron energy spectrum. We assume that the energy density in magnetic fields and in relativistic electrons are fixed fractions ξ_B and ξ_e of the total internal energy density. The magnetic field strength B follows immediately:

$$B = \sqrt{8\pi\xi_B u_i}. \quad (21)$$

(N.b., we use the notation of Paczyński & Rhoads 1993. Some other authors have instead defined ξ_B in terms of the magnetic field strength, such that $B \propto \xi_B$ in their models; care must therefore be taken in comparing scaling laws under these alternative notations.)

The electron energy spectrum requires additional assumptions. We first follow Waxman's (1997a,b) assumptions, to facilitate comparison of our results for beamed bursts with his for unbeamed bursts. In the frame of the expanding blast wave, the swept-up ambient medium

appears as a relativistic wind having Lorentz factor Γ . We assume that the electrons from the ambient medium have their direction of motion randomized in the blast wave frame. Moreover, they may achieve some degree of equipartition with the protons. The typical random motion Lorentz factor γ_e for the swept-up electrons in the blast wave frame is then in the range $\Gamma \lesssim \gamma_e \lesssim 0.5(m_p/m_e)\Gamma$. In terms of the energy density fraction in electrons, $\langle\gamma_e\rangle \approx \xi_e(m_p/m_e)\Gamma$. We further assume that the electrons in the original ejecta mass are not heated appreciably, so that the number of relativistic electrons is $N_e = fM_0/(\mu_e m_p)$ (where μ_e is the mean molecular weight per electron) rather than $(1+f)M_0/(\mu_e m_p)$. We take the electron energy \mathcal{E} to be distributed as a power law $N(\mathcal{E}) = \mathcal{E}^{-p}$ for $\mathcal{E}_{\min} < \mathcal{E} < \mathcal{E}_{\max}$, where $N(\mathcal{E})d\mathcal{E}$ is the number of electrons with energies between \mathcal{E} and $\mathcal{E} + d\mathcal{E}$. Finally, we assume that $p > 2$, so that the total electron energy $\int_{\mathcal{E}_{\min}}^{\mathcal{E}_{\max}} \mathcal{E} N(\mathcal{E}) d\mathcal{E}$ is dominated by electrons with $\mathcal{E} \approx \mathcal{E}_{\min}$, and $\gamma_{e,\text{peak}} \approx \langle\gamma_e\rangle \approx \xi_e(m_p/m_e)\Gamma \approx \mathcal{E}_{\min}/(m_e c^2)$.

The optical depth to synchrotron self-absorption is assumed to be small at the characteristic synchrotron frequency corresponding to $\mathcal{E}_{\min} = \gamma_{e,\text{peak}} m_e c^2$. In the comoving frame, this frequency is $\nu_{co,m} = 0.29 \times 3/(4\pi) \langle \sin \alpha \rangle \gamma_{e,\text{peak}}^2 eB/(m_e c) = 0.29 \times (3/16) \gamma_{e,\text{peak}}^2 eB/(m_e c)$ (Pacholczyk 1970, Rybicki & Lightman 1979), where the calculation of the mean pitch angle $\langle \sin \alpha \rangle = \pi/4$ assumes an isotropic distribution of electron velocities and a tangled magnetic field. Wijers & Galama (1998) have integrated over the power law distribution of electron energies to show that the peak comoving frame frequency for a power law energy distribution becomes $\langle \nu_{co,m} \rangle_{\mathcal{E}} = 3x_p/(4\pi) \times \gamma_{e,\text{peak}}^2 eB/(m_e c)$, where x_p is a function of the power law index p , and where $0.64 \gtrsim x_p \gtrsim 0.45$ for $2 < p < 3$. Below this peak frequency, the flux density rises as $\nu^{1/3}$, while at higher frequencies it falls as $\nu^{-\alpha}$ where $\alpha = (p-1)/2$ (e.g., Rybicki & Lightman 1979, Pacholczyk 1970). Three additional breaks may occur, corresponding to the highest electron energy attained in the shock, the electron energy above which cooling is important, and the frequency where synchrotron self-absorption becomes important. We will comment on the cooling break below, and will ignore the other two breaks for the present.

We first estimate the observer-frame frequency $\nu_{\oplus,m}$ at which the spectrum peaks. This is

$$\begin{aligned} \nu_{\oplus,m} &\approx \langle 1 + \beta \cos(\theta) \rangle_{\theta} \Gamma \times \langle \nu_{co,m} \rangle_{\mathcal{E}} / (1+z) \\ &\approx \frac{1}{1+z} \times \frac{4\Gamma}{3} \times \frac{3x_p}{4\pi} \times \frac{\gamma_{e,\text{peak}}^2 eB}{m_e c} \\ &\approx \frac{1}{1+z} \frac{x_p}{\pi} \left(\xi_e \frac{m_p}{m_e} \right)^2 \frac{eB}{m_e c} \Gamma^3 \end{aligned} \quad (22)$$

where the factor $\langle 1 + \beta \cos(\theta) \rangle_{\theta}$ is the Lorentz transformation for frequency, and where $\beta = \sqrt{1 - \Gamma^{-2}}$ is the expansion velocity as a fraction of lightspeed c . θ is the angle between the velocity vector of radiating material and the photon emitted, as measured in the frame of the emitting matter. $\langle 1 + \beta \cos(\theta) \rangle$ denotes an average weighted by the received intensity. We shall use the highly relativistic limit $\beta \rightarrow 1$ throughout this work, which leads to

the result $\langle 1 + \beta \cos(\theta) \rangle = 4/3$ applied in the final lines of equation 22 (Wijers & Galama 1998).

We estimate the peak flux density following equations 19 and 25 of Wijers & Galama (1998). The basic equation is

$$F_{\nu, m, \oplus} = \Gamma \times N_e \times \phi_p \frac{\sqrt{3}e^3 B}{m_e c^2} \times \frac{1+z}{\Omega_\gamma d^2}. \quad (23)$$

Here $\phi_p \sqrt{3}e^3 B / (m_e c^2)$ is the average comoving frame peak luminosity per unit frequency emitted by a single electron. The details of the average over pitch angle and electron energy are hidden in the factor ϕ_p , which is a function of the electron energy distribution index p with range $0.59 \lesssim \phi_p \lesssim 0.66$ for $2 < p < 3$ (Wijers & Galama 1998). The factor Γ accounts for the Lorentz transformation of flux density (Wijers & Galama 1998). Distance and beaming effects enter through the factor $1/(\Omega_\gamma d^2)$, where d is the luminosity distance to the burst, and Ω_γ is the solid angle into which radiation is beamed. Finally, redshift affects the flux density by factor $(1+z)$ (e.g. Weedman 1986). Our goal is to express $F_{\nu, m, \oplus}$ purely in terms of the dynamical variables we calculated in section 2.

The comoving frame synchrotron cooling time is

$$t_s = \frac{6\pi m_e c}{\sigma_T \gamma_e B^2} \approx \frac{6\pi m_e c}{\sigma_T \gamma_{e, \text{peak}} B^2}, \quad (24)$$

where $\sigma_T = 0.665 \times 10^{-24} \text{ cm}^2$ is the Thompson cross-section (e.g., Rybicki & Lightman 1979).

To obtain the magnetic field strength B , we need the volume of the ejecta cloud, which will have transverse radius $\sim r\zeta_m + c_s t_{co}$ and thickness $\sim c_s t_{co}$, giving comoving volume $V = \pi(ct\zeta_m + c_s t_{co})^2 (c_s t_{co})$. Under the approximation of negligible radiative losses, the internal energy is given by $E_{i, co} = E_0/\Gamma$. The comoving frame magnetic field strength is thus

$$B = \left(\frac{8\xi_B E_0}{\Gamma(ct\zeta_m + c_s t_{co})^2 (c_s t_{co})} \right)^{1/2}. \quad (25)$$

The remaining pieces are trivial. $\Omega_\gamma \approx \pi(\zeta_m + 1/\Gamma)^2$, and d and $1+z$ are simply scale factors.

We now have all the pieces of equations 22 and 23 expressed in terms of dynamical variables from section 2. This means that we can insert these formulae into our numerical integration code and calculate $F_{\nu, m, \oplus}$ and $\nu_{\oplus, m}$ as a function of t_{\oplus} (or of f , Γ , or r). In order to determine a light curve at fixed observed frequency, we combine the broken power law spectral shape described above with the calculated frequency and flux density of the spectral peak to determine the approximate flux density at the observed frequency and time.

The cooling break and self absorption break (cf. Sari, Piran, & Narayan 1998) are additional observed features in afterglow data. We do not treat either in detail here, but do we present a derivation of the cooling break behavior for beamed gamma ray bursts elsewhere (Rhoads 1999b). These results are summarized below. We have not yet treated the self-absorption break. Self-absorption is important primarily at low frequencies, where scintillation can hamper light curve slope measurements. For a treatment of this regime in beamed bursts, see Sari, Piran, & Halpern (1999).

Finally, we consider the evolution of the apparent angular size θ . In the spherical case or the power-law regime for a beamed burst, $\theta = r/(\Gamma d_\theta) \propto t_{\oplus}^{5/8}$ (where d_θ is the angular diameter distance to the burst). In the exponential regime, θ is determined by the physical transverse size of the ejecta cloud rather than the beaming angle, but the difference is not dramatic because the physical size increases at $c_s \sim c$. The result is therefore $\theta \approx c_s t_{co}/d_\theta \propto 1/\Gamma \propto t_{\oplus}^{1/2}$. There is also an intermediate regime, valid for the brief time when $1/\Gamma \gtrsim \zeta_m \gtrsim (c_s t_{co})/(ct)$. In this case, $\theta \propto \zeta_m r \propto t_{\oplus}^{1/4}$. If the exponential regime did not happen at all, this behavior would continue for all $\Gamma < 1/\zeta_m$.

3.2. Analytic Results: Optically thin case

In the limiting cases where one of the terms in the transverse size $\zeta_m ct + c_s t_{co}$ is dominant and the other negligible, we can derive analytic expressions for $F_{\nu, m, \oplus}$ and $\nu_{\oplus, m}$ as functions of observed time t_{\oplus} and the physical parameters of the fireball. We begin with the early time case, and show that its light curve is observationally indistinguishable from that of an isotropic burst.

3.2.1. Power Law Regime

We first determine the comoving magnetic field in this regime by inserting $\zeta_m ct \gg c_s t_{co}$ into equation 25 to obtain

$$B = \frac{2^{1/4} \sqrt{5} \pi c^{7/8}}{3^{3/8} c_s^{1/2} \xi_B} \xi_B^{1/2} \left(\frac{E_0}{\pi \zeta_m^2} \right)^{1/8} \left(\frac{\rho(1+z)}{t_{\oplus}} \right)^{3/8}. \quad (26)$$

Inserting this result into equation 22, we find

$$\begin{aligned} \nu_{\oplus, m} &= \frac{2^{1/4} 5^{1/2}}{3^{3/8} \pi^{1/2}} x_p \xi_e^2 \xi_B^{1/2} \left(\frac{m_p}{m_e} \right)^2 \frac{e}{m_e c^{1/8} c_s^{1/2}} \\ &\times \left(\frac{E_0}{\pi \zeta_m^2} \right)^{1/8} \left(\frac{\rho}{t_{\oplus}} \right)^{3/8} \Gamma^3 (1+z)^{-5/8} \quad (27) \\ &= \frac{5^{1/2}}{2^{7/2}} x_p \xi_e^2 \xi_B^{1/2} \left(\frac{m_p}{m_e} \right)^2 \frac{e}{m_e c^2 c_s^{1/2}} \\ &\times \left(\frac{E_0}{\pi \zeta_m^2} \right)^{1/2} t_{\oplus}^{-3/2} (1+z)^{1/2} \quad (28) \end{aligned}$$

where we have used equation 11 to eliminate Γ in the last line.

For the cooling break, we obtain $\nu_{\oplus, \text{cool}} \propto t_{\oplus}^{-1/2}$ (Rhoads 1999b; Sari et al 1999).

Turning our attention to $F_{\nu, m, \oplus}$, we first need the number N_e of radiating electrons in terms of t_{\oplus} . For the power law regime, this becomes

$$N_e = \frac{2^{3/2}}{3^{1/4}} \frac{(\pi \zeta_m^2 \rho)^{1/4}}{\mu_e m_p} \left(\frac{E_0 t_{\oplus}}{c(1+z)} \right)^{3/4}. \quad (29)$$

Combining this with equations 23, 26, and the appropriate limiting form of Ω_γ , we find

$$F_{\nu, m, \oplus} = \sqrt{10} \pi \frac{\phi_p \xi_B^{1/2}}{\mu_e m_p} \frac{e^3}{m_e c^3} \sqrt{\frac{c}{c_s}} \frac{\rho^{1/2} E_0}{\pi \zeta_m^2} \frac{1+z}{d^2}. \quad (30)$$

Note that this result is independent of t_{\oplus} .

Apart from small differences in the numerical coefficients, our results for the power law regime are essentially the same as the results that Waxman (1997a,b) and Wijers and Galama (1998) obtained for isotropic bursts. Differences between our results and Waxman's are primarily because we have adopted the more precise treatment of the synchrotron peak frequency presented by Wijers and Galama (1998), while differences between our results and those of Wijers and Galama stem from a slightly different way of calculating the comoving frame magnetic field.

3.2.2. Exponential Regime

When $c_s t_{co} \gg \zeta_m c t$, we are in the regime where Γ , t_{\oplus} , etc. all behave exponentially with radius (section 2.2.2). We first rewrite the scalings from equation 20 as

$$\begin{aligned} t_{\oplus}/t_{\oplus,b} &= \exp\{2(r-r_b)/r_{\Gamma}\} \\ f/f_b &= \exp\{2(r-r_b)/r_{\Gamma}\} = t_{\oplus}/t_{\oplus,b} \\ \Gamma/\Gamma_b &= \exp\{-(r-r_b)/r_{\Gamma}\} = (t_{\oplus}/t_{\oplus,b})^{-1/2} \\ t_{co}/t_{co,b} &= \exp\{(r-r_b)/r_{\Gamma}\} = (t_{\oplus}/t_{\oplus,b})^{+1/2}. \end{aligned} \quad (31)$$

We next determine the comoving frame magnetic field in the appropriate limit:

$$B = \left(\frac{8\xi_B E_0}{c_s^3} \right)^{1/2} \Gamma_b^{-1/2} t_{co,b}^{-3/2} \left(\frac{t_{\oplus}}{t_{\oplus,b}} \right)^{-1/2}. \quad (32)$$

Combining this result with equation 22 allows us to determine the peak frequency as

$$\begin{aligned} \nu_{\oplus,m} &= \frac{1}{1+z} \frac{2^{3/2}}{\pi} x_p \xi_e^2 \xi_B^{1/2} \left(\frac{m_p}{m_e} \right)^2 \frac{e}{m_e c} \\ &\times E_0^{1/2} \Gamma_b^{5/2} (c_s t_{co,b})^{-3/2} \left(\frac{t_{\oplus}}{t_{\oplus,b}} \right)^{-2}. \end{aligned} \quad (33)$$

Substituting for the exponential regime initial conditions from equations 16–19 then yields

$$\begin{aligned} \nu_{\oplus,m} &= \frac{1}{1+z} \frac{2^{11/2}}{3^{1/2} 5^{7/2} \pi^{1/2}} x_p \xi_e^2 \xi_B^{1/2} \left(\frac{m_p}{m_e} \right)^2 \\ &\times \frac{e}{m_e} \left(\frac{c_s}{c} \right)^{7/2} \frac{\rho^{1/2}}{\zeta_m^4} \left(\frac{t_{\oplus}}{t_{\oplus,b}} \right)^{-2} \\ &= (1+z) \frac{3^{1/6} 5^{11/6}}{2^{13/2} \pi^{7/6}} x_p \xi_e^2 \xi_B^{1/2} \left(\frac{m_p}{m_e} \right)^2 \\ &\times \frac{e}{m_e} \left(\frac{c_s}{c} \right)^{3/2} \frac{E_0^{2/3}}{\rho^{1/6} c_s^{10/3}} t_{\oplus}^{-2}. \end{aligned} \quad (34)$$

The observed cooling break frequency ceases to evolve in this regime: $\nu_{\oplus,cool} \propto t_{\oplus}^0$ (Rhoads 1999b; Sari et al 1999).

Turning now to the amplitude of the spectral peak, we combine

$$N_e = \frac{25}{8} \frac{E_0 \zeta_m^2}{c_s^2 \mu_e m_p} \frac{t_{\oplus}}{t_{\oplus,b}} \quad (36)$$

and

$$\Omega_{\gamma} = \pi \Gamma^{-2} = \pi \Gamma_b^{-2} (t_{\oplus}/t_{\oplus,b}) \quad (37)$$

with equations 23 and 32 to obtain

$$\begin{aligned} F_{\nu,m,\oplus} &= \frac{3^{1/2} 5^2}{2^{3/2} \pi} \phi_p \xi_B^{1/2} \frac{e^3}{m_e m_p \mu_e} \frac{E_0^{3/2} \zeta_m^2}{c^2 c_s^2} \\ &\times (c_s t_{co,b})^{-3/2} \Gamma_b^{5/2} \left(\frac{t_{\oplus}}{t_{\oplus,b}} \right)^{-1} \frac{1+z}{d^2}. \end{aligned} \quad (38)$$

Substituting the initial conditions for the exponential regime, this becomes

$$\begin{aligned} F_{\nu,m,\oplus} &= \sqrt{\frac{32\pi}{125}} \phi_p \xi_B^{1/2} \frac{e^3}{c^3 m_p m_e \mu_e} \left(\frac{c_s}{c} \right)^{3/2} \\ &\times \frac{E_0 \sqrt{\rho}}{\pi \zeta_m^2} \left(\frac{t_{\oplus}}{t_{\oplus,b}} \right)^{-1} \frac{1+z}{d^2} \\ &= \frac{3^{1/3} 5^{7/6}}{2^{7/2} \pi^{5/6}} \phi_p \xi_B^{1/2} \frac{e^3}{c^3 m_p m_e \mu_e} \left(\frac{c_s}{c} \right)^{1/2} \\ &\times \frac{E_0^{4/3} \rho^{1/6} (1+z)^2}{c_s^{5/3}} \frac{1}{d^2} t_{\oplus}^{-1}. \end{aligned} \quad (40)$$

At $t_{\oplus} = t_{\oplus,b}$, equations 34 and 40 differ from equations 28 and 30 by factors of order unity. This difference is not worrying since our analytic approximations are not expected to be particularly accurate in the transition between the two limiting cases. Numerical correction factors to the coefficients of equations 34 and 40 can be derived from numerical integrations. Such factors are presented in section 3.2.5 below.

3.2.3. TV Dinner Equations

We now pause a moment to consolidate our results so far and express the key equations in terms of fiducial parameter values². We begin with equations 28 and 30. These become

$$\begin{aligned} \nu_{\oplus,m} &= 9.6 \times 10^{12} \times (1+z)^{1/2} \left(\frac{c_s}{c/\sqrt{3}} \right)^{-1/2} \\ &\times \left(\frac{x_p}{0.525} \right) \left(\frac{\xi_e}{0.1} \right)^2 \left(\frac{\xi_B}{0.1} \right)^{1/2} \\ &\times \left(\frac{E_0/10^{53} \text{ erg}}{\zeta_m^2/4} \right)^{1/2} \left(\frac{t_{\oplus}}{\text{day}} \right)^{-3/2} \text{ Hz} \end{aligned} \quad (42)$$

and

$$\begin{aligned} F_{\nu,m,\oplus} &= 11 \times (1+z) \left(\frac{\phi_p}{0.63} \right) \left(\frac{c_s}{c/\sqrt{3}} \right)^{-1/2} \\ &\times \left(\frac{\xi_B}{0.1} \right)^{1/2} \left(\frac{1.3}{\mu_e} \right) \left(\frac{E_0/10^{53} \text{ erg}}{\zeta_m^2/4} \right) \\ &\times \left(\frac{\rho}{10^{-24} \text{ g/cm}^3} \right)^{1/2} \left(\frac{d}{4.82 \text{ Gpc}} \right)^{-2} \text{ mJy}. \end{aligned} \quad (43)$$

²We call these ‘‘TV dinner equations’’ because numerical values for physical constants have been inserted, so they are ready to use without further preparation.

The observed time corresponding to the transition between the power law and exponential regimes is

$$t_{\oplus,b} = 12.1 \times (1+z) \left(\frac{c_s}{c/\sqrt{3}} \right)^{-8/3} \left(\frac{E_0/10^{53} \text{ erg}}{\zeta_m^2/4} \right)^{1/3} \\ \times \left(\frac{\rho}{10^{-24} \text{ g/cm}^3} \right)^{-1/3} \left(\frac{\zeta_m}{0.1} \right)^{8/3} \text{ days} . \quad (44)$$

Thereafter, the frequency and flux density at the spectral peak are characterized by equations 28 and 40. Numerical integrations show that modest correction factors $\epsilon_\nu \approx 0.74$ and $\epsilon_F \approx 0.7$ should be applied to these two equations at late times to compensate for approximations in the initial conditions (see section 3.2.4 below). These have been incorporated in the following three equations.

The observed frequency of the spectral peak at the time of the break is

$$\nu_{\oplus,m,b} = \frac{1.7 \times 10^{11}}{1+z} \left(\frac{\epsilon_\nu}{0.74} \frac{x_p}{0.525} \right) \left(\frac{c_s}{c/\sqrt{3}} \right)^{7/2} \\ \times \left(\frac{\xi_e}{0.1} \right)^2 \left(\frac{\xi_B}{0.1} \right)^{1/2} \left(\frac{\rho}{10^{-24} \text{ g/cm}^3} \right)^{1/2} \left(\frac{\zeta_m}{0.1} \right)^{-4} \text{ Hz} . \quad (45)$$

The subsequent evolution is given by

$$\nu_{\oplus,m} = \nu_{\oplus,m,b} \times \left(\frac{t_{\oplus}}{t_{\oplus,b}} \right)^{-2} \quad (46)$$

and

$$F_{\nu,m,\oplus} = 0.41 \times \left(\frac{\epsilon_F}{0.7} \frac{\phi_p}{0.63} \right) \left(\frac{c_s}{c/\sqrt{3}} \right)^{3/2} \left(\frac{\xi_B}{0.1} \right)^{1/2} \\ \times \left(\frac{1.3}{\mu_e} \right) \left(\frac{E_0/\zeta_m^2}{10^{53} \text{ erg}/4} \right) \left(\frac{\rho}{10^{-24} \text{ g/cm}^3} \right)^{1/2} \\ \times (1+z) \left(\frac{d}{4.82 \text{ Gpc}} \right)^{-2} \left(\frac{t_{\oplus}}{t_{\oplus,b}} \right)^{-1} \text{ mJy} . \quad (47)$$

Finally, for completeness, we include our result for $\nu_{\oplus,\text{cool}}$ from Rhoads 1999b:

$$\nu_{\oplus,\text{cool}} = \left[5.89 \times 10^{13} (t_{\oplus}/t_{\oplus,b})^{-1/2} + 1.34 \times 10^{14} \right] \text{ Hz} \\ \times \left(\frac{1}{1+z} \right) \left(\frac{c_s}{c/\sqrt{3}} \right)^{17/6} \left(\frac{\xi_B}{0.1} \right)^{-3/2} \\ \times \left(\frac{\rho \cdot \text{cm}^3}{10^{-24} \text{ g}} \right)^{-5/6} \left(\frac{E_0/10^{53} \text{ erg}}{\zeta_m^2/4} \right)^{-2/3} \left(\frac{\zeta_m}{0.1} \right)^{-4/3} . \quad (48)$$

Note that this equation already interpolates over the break time $t_{\oplus,b}$; the interpolation was derived in the fashion suggested in section 3.2.5 below.

3.2.4. Putting the Pieces Together

An accurate description of the behavior in the transition between the power law and exponential regimes can be obtained numerically. We first note that there is a single characteristic observed time $t_{\oplus,b}$ given by equation 18 and flux level $F_{\nu,m,\oplus,b} \equiv F_{\nu,m,\oplus}(t_{\oplus} \ll t_{\oplus,b})$ given by equation 30. If we use these as our basic time and flux units,

and denote the observed time and peak flux scaled to these units as $\widehat{t_{\oplus}}$ and $\widehat{F_{\nu,m,\oplus}}$, there is a unique $\widehat{F_{\nu,m,\oplus}}(\widehat{t_{\oplus}})$ relation. This is plotted in figure 2.

Similarly, we can define the characteristic frequency $\nu_{\oplus,m,b}$ in the problem to be given by equation 28 evaluated at $t_{\oplus,b}$, and $\widehat{\nu_{\oplus,m}}$ to be the frequency scaled by this value. Then we can again obtain a unique relation $\widehat{\nu_{\oplus,m}}(\widehat{t_{\oplus}})$, which is shown in figure 3.

At late times, the numerical integrations yield a flux density that is a factor $\epsilon_F \approx 0.7$ smaller than in equation 40, and a frequency of peak emission that is a factor $\epsilon_\nu \approx 0.74$ smaller than in equation 34. This is presumably due to the approximate initial conditions used for the exponential regime evolution. These initial conditions are obtained by applying an asymptotic approximation outside its range of validity, and it should not be surprising if this procedure introduces some error. We suggest below that this error may be corrected empirically.

To obtain predictions for a given set of model parameters from these dimensionless curves, we need only (1) determine numerically the values of $t_{\oplus,b}$, $F_{\nu,m,\oplus,b}$, and $\nu_{\oplus,m,b}$; and (2) determine the time interval over which our assumption $1/\Gamma_0 \lesssim f \lesssim \Gamma_0$ remains valid. The early behavior, before the ejecta accrete a dynamically important amount of ambient medium (i.e., $f < 1/\Gamma_0$) is unlikely to be observed at long wavelengths, since it is over within a fraction of a second for reasonable burst parameters. We therefore consider only the end condition, $f \approx \Gamma_0$. This happens at $t_{\oplus} = t_{\oplus,f}$, where

$$t_{\oplus,f} \approx \Gamma_0 t_{\oplus,b} / f_b \approx \frac{8}{25} \left(\frac{c_s}{c} \right)^2 \frac{1}{\zeta_m^2} t_{\oplus,b} . \quad (49)$$

At later times, our assumptions that $\Gamma \gtrsim 2$ and $\beta \approx 1$ break down, and the behavior of the fireball changes again. Such changes may be relevant to the radio behavior of gamma ray burst afterglows, but we will not consider them here.

3.2.5. Empirical Interpolations

To obtain a readily calculated burst behavior around time $t_{\oplus,b}$, we can interpolate between the asymptotic behaviors for earlier and later times. We do this first for $F_{\nu,m,\oplus}$ and then for $\nu_{\oplus,m}$. We use interpolants of the form $g = (g_1^{-\kappa} + \epsilon g_2^{-\kappa})^{-1/\kappa}$, where g_1 and ϵg_2 represent limiting behaviors of an arbitrary function g for early and late times. The exponent κ determines the smoothness of the transition between the limiting behaviors. The scalar ϵ is introduced so that the numerically derived correction factors to the late-time asymptotic results can be applied.

For $F_{\nu,m,\oplus}$, the asymptotic behaviors are $F_{\nu,m,\oplus}$ constant and $F_{\nu,m,\oplus} \sim \widehat{t_{\oplus}}^{-1}$. We work with the scaled quantities defined in section 3.2.4, so that the break between the two asymptotic behaviors is expected for $\log(\widehat{t_{\oplus}}) \sim 0$. We set $g_1 = F_{\nu,m,\oplus,b}$. We use equation 40 for g_2 , and set the correction factor $\epsilon = 0.7$. Finally, we choose $\kappa = 0.4$. The resulting interpolation is plotted atop the numerical integration results in figure 2.

The asymptotic behaviors of $\nu_{\oplus,m}$ are $\propto t_{\oplus}^{-3/2}$ and $\propto t_{\oplus}^{-2}$. In this case, we have taken g_1 from equation 28. For g_2 , we take equation 34, and set $\epsilon = 0.74$. Here we

find $\kappa = 5/6$ works well. This interpolation is shown in figure 3.

3.2.6. Light Curves: Optically thin case

The afterglow light curve at fixed observed frequency is obtained by combining the predicted behavior of $\nu_{\oplus,m}$ and $F_{\nu,m,\oplus}$ with the spectrum for a truncated power law electron energy distribution. We use the analytic results of section 3.2. Then we find four generic behaviors, depending on whether the frequency is above or below $\nu_{\oplus,m}$ and whether the time is earlier or later than $t_{\oplus,b}$. These are

$$F_{\nu,\oplus} \propto \begin{cases} t_{\oplus}^{1/2} & t_{\oplus} < t_{\oplus,b}; \quad \nu_{\oplus} < \nu_{\oplus,m}(t_{\oplus}) \\ t_{\oplus}^{-3(p-1)/4} & t_{\oplus} < t_{\oplus,b}; \quad \nu_{\oplus} > \nu_{\oplus,m}(t_{\oplus}) \\ t_{\oplus}^{-1/3} & t_{\oplus} > t_{\oplus,b}; \quad \nu_{\oplus} < \nu_{\oplus,m}(t_{\oplus}) \\ t_{\oplus}^p & t_{\oplus} > t_{\oplus,b}; \quad \nu_{\oplus} > \nu_{\oplus,m}(t_{\oplus}) \end{cases} \quad (50)$$

Here p is the electron energy spectrum slope and $\alpha = (p-1)/2$ is the high frequency spectral slope, as usual. Note particularly how steep the light curve becomes for $t_{\oplus} > t_{\oplus,b}$ and $\nu_{\oplus} > \nu_{\oplus,m}(t_{\oplus})$.

Three representative light curves are shown in figure 4. These have been derived by combining the empirically interpolated $\widehat{\nu_{\oplus,m}}$ and $\widehat{F_{\nu,m,\oplus}}$ curves with the broken power law spectrum. Note that the rollover at the beaming transition ($\log(\widehat{t_{\oplus}}) \sim 0$) is rather slow, so that observed behavior will be intermediate between the asymptotic power laws of equations 50 for a considerable time. This slow rollover is in part due to the compound nature of the break. The light curve decay begins to accelerate as soon as we can “see” the edge of the jet, when $\Gamma < 1/\zeta_m$. The additional steepening when dynamical effects of beaming become important occurs slightly later, when $\Gamma < \Gamma_b \sim 0.23/\zeta_m$ (cf. equation 17) (cf. Panaitescu & Mészáros 1999 for additional discussion of this point).

Equation 50 assumes $\nu_{\oplus,abs} < \nu_{\oplus} < \nu_{\oplus,cool}$ throughout. (Here $\nu_{\oplus,abs}$ is the self-absorption frequency, measured in the observer’s frame.) If we now include the cooling break, we obtain the additional light curve behaviors (derived in Rhoads 1999b)

$$F_{\nu,\oplus} \propto \begin{cases} t_{\oplus}^{1/2-3p/4} & t_{\oplus} < t_{\oplus,b}; \quad \nu_{\oplus} > \nu_{\oplus,cool}(t_{\oplus}) \\ t_{\oplus}^{-p} & t_{\oplus} > t_{\oplus,b}; \quad \nu_{\oplus} > \nu_{\oplus,cool}(t_{\oplus}) \end{cases} \quad (51)$$

where we have also assumed that $\nu_{\oplus,m} < \nu_{\oplus,cool}$. These behaviors are not shown in figure 4, but were used to fit the light curve of GRB 970508 with beamed afterglow models (Rhoads 1999b).

3.2.7. Light Curves: Optically thin case without sideways expansion

It remains possible to constrain gamma ray burst beaming by looking for light curve breaks even in the case where lateral expansion of the evolving burst remnant is unimportant. This corresponds to dropping our fourth assumption from section 2.

In this case, the dynamical evolution follows power law behavior (section 2.2.1) throughout, but the emergent radiation is diluted relative to the spherical case by a factor

$\Gamma^2 \zeta_m^2$ once $\Gamma < 1/\zeta_m$. For an adiabatic evolution, we have $\Gamma^2 \propto t_{\oplus}^{-3/4}$. The power law exponents for the light curve in this regime become $-1/4$ for $\nu_{\oplus,abs} < \nu < \nu_{\oplus,m}$, $-3p/4$ for $\nu_{\oplus,m} < \nu < \nu_{\oplus,cool}$, and $-1/4 - 3p/4$ for $\nu_{\oplus,cool} < \nu$.

The most plausible mechanism for quenching lateral expansion is a strongly radiative remnant, so it is more relevant to examine this regime with radiative dynamics. Then $\Gamma^2 \propto t_{\oplus}^{-6/7}$, and all the light curve exponents decrease by an additional $3/28$, becoming $-5/14$ for $\nu_{\oplus,abs} < \nu < \nu_{\oplus,m}$, $-3/28 - 3p/4$ for $\nu_{\oplus,m} < \nu < \nu_{\oplus,cool}$, and $-5/14 - 3p/4$ for $\nu_{\oplus,cool} < \nu$.

While these slope changes are less dramatic than those in section 3.2.6, they would be strong enough to detect in afterglow light curves with reasonably large time coverage and good photometric accuracy.

3.3. Optically Thick Case

We now consider briefly the electron energy distribution model of Paczyński & Rhoads (1993). This model differs from that of the preceding sections in a few ways. First, the electron power law index was fixed at $p = 2$ to avoid strong divergences in the total energy density in electrons. Second, the minimum electron energy \mathcal{E}_{min} was taken to be sufficiently small that emission from electrons with $\mathcal{E} = \mathcal{E}_{min}$ was always in the optically thick regime. Under these circumstances, there is a single break in the electron energy spectrum at the frequency corresponding to optical depth $\tau = 0.35$ (cf. Pacholczyk 1970), with spectral slope $\nu^{5/2}$ below the break and $\nu^{-1/2}$ above. The magnetic field behavior is the same in this model and more recent ones.

Combining this electron behavior with the power law regime dynamical model reproduces the scalings from Paczyński & Rhoads (1993), namely

$$\nu_{\oplus,m} \propto E_0^{1/3} \rho^{1/3} t_{\oplus}^{-2/3} \quad (52)$$

and

$$F_{\nu,\oplus,m} \propto E_0^{7/8} \rho^{1/8} \nu_{\oplus,m}^{5/8} \propto E_0^{13/12} \rho^{1/3} t_{\oplus}^{-5/12} \quad (53)$$

If we use instead the exponential regime dynamical model, we find

$$\nu_{\oplus,m} \propto t_{\oplus}^{-1} \quad \text{and} \quad F_{\nu,\oplus,m} \propto t_{\oplus}^{-3/2} \quad (54)$$

Readers interested in the precise numerical coefficients for these relations are referred to Paczyński & Rhoads (1993) for the spherical case. For the beamed case, numerical results may be found by applying the Paczyński & Rhoads (1993) results at the transition between the power law and exponential regimes, and continuing the evolution using equations 54.

The light curve for this electron model then becomes

$$F_{\nu,\oplus} \propto \begin{cases} t_{\oplus}^{5/4} & t_{\oplus} < t_{\oplus,b}; \quad \nu_{\oplus} < \nu_{\oplus,m}(t_{\oplus}) \\ t_{\oplus}^{-3/4} & t_{\oplus} < t_{\oplus,b}; \quad \nu_{\oplus} > \nu_{\oplus,m}(t_{\oplus}) \\ t_{\oplus}^1 & t_{\oplus} > t_{\oplus,b}; \quad \nu_{\oplus} < \nu_{\oplus,m}(t_{\oplus}) \\ t_{\oplus}^{-2} & t_{\oplus} > t_{\oplus,b}; \quad \nu_{\oplus} > \nu_{\oplus,m}(t_{\oplus}) \end{cases} \quad (55)$$

The behavior here at frequencies $\nu_{\oplus} > \nu_{\oplus,m}(t_{\oplus})$ is the same as in equations 50 with $p = 2$. However, $\nu_{\oplus,m}$ has a different meaning in the two models.

From these results, we see that the substantial changes in the observable behavior of a beamed burst are not dependent on the precise nature of the electron energy distribution.

4. DISCUSSION

We now put mathematics aside to recapitulate our results and to discuss their implications for the interpretation of afterglow observations.

We have shown that the dynamics of a gamma ray burst remnant change qualitatively when the remnant's Lorentz factor Γ drops below the reciprocal opening angle $1/\zeta_m$ of the ejecta. Before this time, the Lorentz factor behaves as a power law in radius. Afterwards, the Lorentz factor decays exponentially with radius. The change occurs because lateral expansion of the ejecta cloud increases the rate at which additional material is accreted. Such lateral expansion is prohibited by symmetry in the spherical case.

When the remnant enters this "exponential regime," the relation between the observed spectrum and the observed light curve changes. Inferences about the electron energy spectrum in afterglows come from the light curve decay rate and spectral slope. The general agreement between the two methods has been taken as a confirmation of the (spherically symmetric) fireball model (Wijers, Rees, & Mészáros 1997; Waxman 1997a).

The light curve decline at frequencies above the spectral peak becomes very steep (t_{\oplus}^{-p} , where p is the index of the electron energy spectrum) once the burst dynamics enter the exponential regime. Reconciling this relation with the observed decays ($-1 \gtrsim d \log(F_{\nu, \oplus})/d \log(t_{\oplus}) \gtrsim -1.5$) would require an extremely flat electron energy spectrum, and consequently a very blue spectral energy distribution. This was not seen in early observed spectral energy distributions (see Wijers et al 1997 for GRB 970228; Reichart 1997 and Sokolov et al 1997 for GRB 970508; and Reichart 1998 for GRB 971214). We infer that GRBs 970228, 970508, and 971214 were probably not in the exponential regime during their observed optical afterglows. GRB 971227 provides a possible, though dubious, counterexample. There is one image suggesting a counterpart (magnitude $R \approx 19.5$) on December 27.91 (Castro-Tirado et al 1997). Later images show no corresponding source, requiring a decay at least as fast as $t_{\oplus}^{-2.5}$ (Djorgovski et al 1998). This is consistent with a t_{\oplus}^{-p} decay for typical values of p . However, this explanation remains speculative, since there is no second image confirming the proposed counterpart.

Subsequent afterglows have provided a more hopeful picture for practical application of beaming models. In particular, GRB 990123 shows a break that is quite possibly due to beaming (e.g., Castro-Tirado et al 1999; Kulkarni et al 1999), and comparison of the spectral slope and decay slope for GRB 980519 gives better agreement for beamed than for spherical regime models (Sari et al 1999).

In the case of GRB 970508, we can place a stringent limit on the beaming angle in the context of our model. The optical light curve extends to ~ 100 days after the burst and does not depart drastically from a single power law after day 2 (Pedersen et al 1998); thus, no transition to the exponential regime occurred during this time. As already noted, the spectral slope and light curve law decay

rate are in fair agreement for the spherical case, and poor agreement for the beamed case. The radio light curve furnishes the last critical ingredient. Goodman (1997) pointed out that diffractive scintillation by the Galactic interstellar medium is expected in early time radio data, and that this scintillation will stop when the afterglow passes a critical angular size. By comparing this characteristic size with the time required for the scintillations to die out, one can measure the burst's expansion rate. This test has been applied (Frail et al 1997; Waxman, Kulkarni, & Frail 1998) and shows that $\Gamma \lesssim 2$ at $t_{\oplus} \sim 14$ days. Thus, no power-law break to faster decline is observed at $\Gamma \gtrsim 2$, and we infer that GRB 970508 was effectively unbeamed ($\zeta_m \gtrsim 1/2$). This rough derivation is borne out by detailed fitting of beamed afterglow models to the GRB 970508 light curve, which yields the same beaming limit $\zeta_m \gtrsim 1/2$ radian (Rhoads 1999b).

This conclusion, combined with the GRB 970508 redshift limit $z \geq 0.835$ (Metzger et al 1997), immediately implies a minimum energy for the burst. This burst was detected as BATSE trigger 6225, and the total BATSE fluence was $(3.1 \pm 0.2) \times 10^{-6}$ erg/cm² over the range 20–1000 keV (Kouveliotou et al 1997). The gamma ray emission alone therefore implies $E_0 \gtrsim 4.7 \times 10^{51} (\Omega/4\pi)$ erg $\gtrsim 3 \times 10^{50}$ erg. Here we have based the luminosity distance on an $\Omega = 0.2$, $\Lambda = 0$, $H_0 = 70$ km/s/Mpc cosmology, and applied the beaming angle limit $\zeta_m \gtrsim 0.5$ radian in the second inequality. This conclusion is of course model-dependent and might change if our assumptions about the blast wave physics or beaming geometry are badly wrong. We will discuss possible ways to reduce the energy requirements of GRB 970508 while retaining consistency with the afterglow data in section 4.1 below.

If the beaming angle ζ_m is substantially variable from burst to burst, it is possible that some bursts enter the rapid decay phase before the spectral peak passes through optical wavelengths. Present data suggests that this is indeed the case; GRB 980519 is best fit by assuming exponential regime behavior (Sari et al 1999), while GRB 990123 appears to be a transition case with a break observed in the optical light curve (e.g. Castro-Tirado et al 1999, Kulkarni et al 1999, Sari et al 1999). The resulting rapid decay could then explain some of the optical non-detections of well studied GRBs such as 970828 (Groot et al 1997). Alternatively, for characteristic beaming angles $1 \gg \zeta_m \gtrsim 0.1$, we would expect beaming to become dynamically important between the time of peak optical and radio afterglow. This would then help explain the paucity of radio afterglows, which unlike optical afterglows cannot be hidden by dust in the burster's environment. There is some evidence that the radio emission involves a different process, or at least a different electron population, from the optical and X-ray afterglows: The peak flux density in GRB 970508 did not follow a single power law with wavelength as it ought to under the simplest fireball models (Katz & Piran 1997b).

The transition in light curve behavior at $\Gamma \sim 1/\zeta_m$ is also important for "blind" afterglow searches. Such searches would look for afterglows not associated with detected gamma ray emission. A much higher event rate for afterglows than for bursts is a natural consequence of beamed fireball models, since the afterglow emission peaks

at lower bulk Lorentz factors than the gamma ray emission does. Comparison of event rates at different wavelengths can therefore constrain the ratio of beaming angles at those wavelengths (Rhoads 1997a). However, we will only see the afterglow if either (a) we are within angle ζ_m of the burst's symmetry axis, and therefore could also see the gamma ray burst, or (b) the Lorentz factor has decayed to $\Gamma < 1/\zeta_m$ and the afterglow light curve has entered its steep decay phase. We have already argued that GRB 970228, GRB 970508, and GRB 971214 were not in this steep decay phase based on the comparison of light curves and spectral slopes. It follows that if blind afterglow searches find a population of afterglows not associated with observed gamma rays, those afterglows will exhibit a steeper light curve decay than did the 1997 afterglows. The efficiency for detecting such rapidly fading "orphan" afterglows will be substantially lower than the efficiency estimated from direct comparison with spherical-regime afterglows.

Other models of beamed gamma ray bursts are possible. In particular, we have assumed a "hard-edged" jet, where the mass and energy emitted per unit solid angle are constant at small angles and drop to zero as a step function at large angles. Profiles in which these quantities decrease smoothly to zero may be more realistic. Whether these differ importantly from the model presented here depends on whether most of the energy is emitted into a central core whose properties vary slowly across the core. Layered jet models in which most of the kinetic energy from the fireball is carried by material with a low Lorentz factor can have substantially different afterglow light curves from either the spherically symmetric case or the hard-edged jet case. This is because the afterglow emission can be dominated by outer layers where the initial Lorentz factor is high enough to yield optical emission during ejecta deceleration, but insufficient to yield gamma rays. The afterglow is thereby effectively decoupled from the gamma ray emission, and it becomes harder to predict one from the other. Such models have been explored by several groups (e.g., Mészáros & Rees 1997b; Mészáros, Rees, & Wijers 1997; Paczyński 1997). A similar decoupling of the gamma-ray and afterglow properties can be produced in the spherical case by allowing inner shells of lower Lorentz factor and larger total mass and energy to follow the initial high- Γ ejecta (Rees & Mészáros 1998).

It is possible to approximate the afterglow from a layered jet by a superposition of hard-edged jets. For this to be reasonably accurate, the outer layers should have Lorentz factors substantially below those of the inner layers, and opening angles and energies substantially above those of the inner layers.

4.1. Energy Requirements for GRB 970508

We now consider how our model will change if we vary some of the basic assumptions. Our primary concern is to determine whether the minimum energy required to power the GRB 970508 afterglow can be reduced substantially below the requirements derived from a spherical adiabatic fireball model expanding into a homogeneous medium. We will therefore sometimes err on the side of extreme model

assumptions chosen to minimize the energy needs. In order to declare a model consistent with the data, we require that either (1) there be no break in the light curve or spectrum around $\Gamma \sim 1/\zeta_m$, or (2) the break occurs early (before $t_{\oplus} \sim 2$ days) and the late time light curve shows a slow decline even for spectral slopes as red as those observed.

The first requirement is physically implausible. Even in the absence of the dynamical effects reported above, so long as the afterglow is from relativistically moving and decelerating material, its flux will scale with an extra factor Γ^2 once $\Gamma \gtrsim 1/\zeta_m$. Since Γ decreases with time, a break is generally expected, though perhaps it could be avoided with sufficient fine-tuning of the model.

The second possibility is more interesting. It requires us to construct a model where factors besides beaming contribute relatively little to the decay of $F_{\nu,m,\oplus}$ with t_{\oplus} , or where the observed spectrum does not directly tell us about the electron energy distribution. A burst expanding into a cavity (such that ρ increases with r) might give a slow decay, while a sufficiently large dust column density would give a red spectrum despite a flat electron energy distribution (cf. Reichart 1997, 1998). However, both would require some degree of fine tuning. The dust-reddened spectra would deviate measurably from pure power-laws given good enough data, but the present data are probably equally consistent with both pure and reddened power law spectra. Certainly such reddened beaming models would imply little correlation between observed spectral slopes and light curve decays, since the dust column density could vary wildly from burst to burst. This hypothesis is somewhat ad hoc, but is consistent with present data and is supported by other circumstantial evidence linking GRBs to dust and star forming regions (e.g. Groot et al 1997; Paczyński 1998). At present, then, it appears the most viable way of reconciling beamed fireball scenarios with the 1997 afterglow data.

We now discuss a few variations of fireball models in greater detail.

4.1.1. Radiative case

We first consider the behavior of a radiative regime fireball. In this regime, the internal energy of the fireball is low, since it is converted to photons and radiated away. The largest implications for beaming are when the internal energy density is so low that $c_s \ll c$. In this case, the lateral expansion that leads to the exponential regime of burst remnant evolution in the adiabatic case is unimportantly small. We assume this low sound speed through much of the following discussion.

We assume that energy in magnetic fields and protons is transferred to electrons in the burst remnant on a remnant crossing time ($\sim t_{co}$). The electrons are assumed to maintain a power law energy spectrum, with a large \mathcal{E}_{\max} whose precise value is determined by the requirement that the burst radiate its internal energy efficiently. Under these circumstances, the Lorentz factor scales as $\Gamma \propto r^{-3}$ and the comoving frame internal energy E_{int} of the remnant follows the evolution

$$\frac{dE_{int}}{dr} \sim \Gamma \rho c^2 \pi \zeta_m^2 r^2 - \frac{E_{int}}{t_{co}} \frac{dt_{co}}{dr} \sim \frac{\pi \rho c^2 \zeta_m^2 (\Gamma r^3)}{r} - \frac{4E_{int}}{r}. \quad (56)$$

This admits a solution of the form $E_{int} \sim (\pi \zeta_m^2 \rho c^2 (\Gamma r^3) - c_2 r^{-4})/4$ where c_2 is a constant of integration. At late times, we throw away the $c_2 r^{-4}$ term, which becomes negligible. The result then becomes

$$E_{int} \approx (\Gamma r^3) \pi \zeta_m^2 \rho c^2 / 4 \quad (57)$$

which is constant since $\Gamma \propto r^{-3}$ in this regime. If the sound speed becomes negligibly small at some point in the burst remnant evolution, then the volume of the shell scales as $V \propto r^2$ thereafter. The magnetic field then scales as $B \propto r^{-1}$, based on constant E_{int} . The observed peak frequency scales as $\nu_{\oplus, m} \propto \Gamma^3 B \propto r^{-10} \propto t_{\oplus}^{-10/7}$.

The power radiated is simply $\sim \Gamma \times (\Gamma - 1) c^2 \times \pi \zeta_m^2 r^2 c \rho$ in the observer's frame, but this is dominated by emission from electrons at \mathcal{E}_{max} , which we have not calculated. The peak in $F_{\nu, \oplus}$ must be estimated as before. We have total comoving frame energy $\sim \xi_e E_{int}$ in electrons at $\mathcal{E} \sim \mathcal{E}_{min}$, which is radiated over the comoving cooling time $t_s \sim 1/(\Gamma B^2) \sim V/(\Gamma E_{int}) \sim r^5$. In the observer frame, this gives total power output $\sim \Gamma^2 E_{int}/t_s$, accounting for factors of Γ from the Lorentz boost to photon energies and for the transformation between t_{co} and t_{\oplus} . The frequency range containing this power scales as $\Delta\nu_{\oplus} \propto \nu_{\oplus, m}$. So, in the spherical case, $F_{\nu, m, \oplus} \propto \Gamma^2 E_{int}/(t_s \nu_{\oplus, m}) \propto r^{-1} \propto t_{\oplus}^{-1/7}$. If we now allow for beaming, we introduce another factor of $\Omega_{\gamma}^{-1} = \Gamma^2/\pi$ and obtain $F_{\nu, m, \oplus} \propto r^{-7} \propto t_{\oplus}^{-1}$.

Finally, putting in the spectral shape for fixed $\nu_{\oplus} > \nu_{\oplus, m}$, we find that $F_{\nu, \oplus} \propto t_{\oplus}^{-(5p+2)/7}$. Thus, this radiative regime model yields scalings fairly similar to our canonical adiabatic model. In particular, the late time light curve again shows a steep decline. While the assumptions made here may not be fully self-consistent, allowing $c_s \sim c$ would likely further steepen this decline.

This result suggests that the GRB 970508 data cannot easily be reconciled with a beamed radiative afterglow model.

4.1.2. Beamed burst, isotropic afterglow

Gamma ray bursters may give rise to both fast and slow ejecta, where ‘‘slow’’ here means too slow to cause gamma ray emission. In this case, the optical and γ -ray properties of the event may be effectively decoupled if the slow wind contains most of the energy.

Suppose the gamma ray burst is caused by a small amount of extremely relativistic ejecta, while the afterglow is caused primarily by a greater mass of material with low Γ_0 . The afterglow light curve places almost no direct constraint on the isotropy of the first (high- Γ_0) material. However, the low- Γ material must be reasonably isotropic to avoid a visible break in the light curve at late time. To explain a peak optical flux of $\sim 30 \mu\text{Jy}$ in the optical, we need total energy

$$E_0 = 1.5 \times 10^{50} \text{ erg} \times \left(\frac{0.63 \mu_e}{\phi_p 1.3} \right) \left(\frac{c_s}{c/\sqrt{3}} \right)^{1/2} \left(\frac{\xi_B}{0.1} \right)^{-1/2} \\ \times \left(\frac{\rho \cdot \text{cm}^3}{10^{-24} \text{ g}} \right)^{-1/2} \left(\frac{1.835}{1+z} \right) \left(\frac{d}{4.82 \text{ Gpc}} \right)^2 \quad (58)$$

(see equations 30 and 43), where we have assumed isotropy and where 4.82 Gpc is the luminosity distance corresponding to $z = 0.835$ for cosmological parameters $\Omega = 0.2$,

$\Lambda = 0$, and $H_0 = 70 \text{ km/s/Mpc}$ (cf. equation 30). We compare this to the optical fluence of the burst, which we estimate as

$$Q_{opt} = \int_0^{\infty} \int_0^{\nu_{max}} F_{\nu, \oplus} d\nu dt_{\oplus} \quad (59)$$

Inserting our broken power law spectrum and the dependence of $\nu_{\oplus, m}$ on t_{\oplus} yields

$$Q_{opt} \approx \left(\frac{2}{3} + \frac{4}{p-7/3} \right) F_{\nu, m, \oplus} \nu_1 t_{\oplus, m}(\nu_1) \left(\frac{\nu_{max}}{\nu_1} \right)^{1/3} \quad (60)$$

Here ν_1 is an arbitrary reference frequency, and $t_{\oplus, m}(\nu_1)$ is defined as the moment when $\nu_{\oplus, m} = \nu_1$. Setting $\nu_1 = 6 \times 10^{14} \text{ Hz}$ (corresponding to wavelength $0.5 \mu\text{m}$), $F_{\nu, m, \oplus} = 30 \mu\text{Jy}$, $t_{\oplus, m}(\nu_1) = 2 \text{ days}$, and $p \approx 2.85$ (corresponding to a $t_{\oplus}^{-1.4}$ light curve) yields $Q_{opt} = 3.0 \times 10^{-7} (\nu_{max}/\nu_1)^{1/3} \text{ erg/cm}^2$. (A similar calculation using $p = 2.2$ and accounting for the additional break at the cooling frequency yields a similar fluence, $3.8 \times 10^{-7} \text{ erg/cm}^2$, for $\nu_{max} = \nu_1 = 6 \times 10^{14} \text{ Hz}$. This is the value used in Rhoads 1999b.) Taking luminosity distance 4.82 Gpc and considering only optical and longer wavelength afterglow, the smaller optical fluence estimate implies $E = 4.5 \times 10^{50} (\Omega/4\pi) \text{ erg} \gtrsim 2.8 \times 10^{49} \text{ erg}$. We have applied our beaming limit, $\zeta_m \gtrsim 0.5$ radian, to derive the lower limit here. If we take ν_{max} corresponding to the soft X-ray afterglow, the energy rises by another factor of ~ 10 . These fluence-based energy needs are dangerously close to exceeding the energy requirements from equation 58. Since the latter equation is based on an energy-conserving model, this comparison shows that ξ_B must be substantially below 1 and/or the density substantially below 10^{-24} g/cm^3 if the model is to be self-consistent. Otherwise, the total energy radiated is comparable to or greater than the total energy available. Reassuringly, the density and magnetic energy fraction found by Wijers & Galama (1998) are roughly consistent with these requirements. This consistency check could be refined by replacing equation 60 with a more detailed fluence calculation.

4.1.3. Layered jet models

In this class of models, considered (for example) by Mészáros, Rees, & Wijers (1997) and Panaitescu, Mészáros, & Rees (1998), the material dominating the emission changes continuously through a range of initial Lorentz factors. We can approximate such models as a superposition of many ‘‘hard-edged’’ jet models. We have tried developing such models while minimizing the energy requirements. To do this, we build a sequence of adiabatic hard-edged jets, enforcing either the condition $\nu_{\oplus, m} = \nu_{\oplus}$ or the condition $t_{\oplus, b} = t_{\oplus}$ throughout the afterglow evolution, and then adjusting the input energy requirement to match the observed light curve. (Here ν_{\oplus} denotes the fixed frequency at which our data was taken.) A preliminary exploration of such models has not yielded any drastic reduction in energy requirements. A more thorough study may be needed to make this conclusion firm.

4.1.4. Inhomogeneous environments

The predictions of fireball models change somewhat if the ambient medium is not uniform. To date, investigations of variable density environments have concentrated on density laws $\rho \propto r^{-g}$ (Vietri 1997b; Mészáros, Rees, & Wijers 1997; Panaitescu, Mészáros, & Rees 1998). The best motivated choices of g are $g = 0$ and $g = 2$, which correspond to a uniform density medium and the density profile expected from a constant speed wind from the burst progenitor expanding into a vacuum (or an ambient medium of much lower density). When the ambient density decreases with increasing distance from the burster, the general result for spherical symmetry is a faster decay of the afterglow flux (e.g. Panaitescu et al 1998) (though the duration of the afterglow should increase correspondingly). We therefore infer that a decreasing density profile will also steepen the light curve decline in the beamed case. This only exacerbates the disagreement between the observed slow afterglow decay and the model predictions for beamed bursts, given the observed spectral energy distribution.

It is worth asking how the exponential regime of burst remnant evolution (section 2.2.2) will change if the ambient density is nonuniform. The exponential scale length $r_r \propto \rho^{-1/3}$ in the uniform density case. We therefore conjecture that a solution similar to the following may be possible:

$$\begin{aligned} \Gamma &\sim \exp \left[- \left(\frac{r}{r_r(\rho_1) \times (\rho/\rho_1)^{-1/3}} \right) \right] \\ &\sim \exp \left[- \left(\frac{r}{r_r(\rho_1) \times (r/r_1)^{g/3}} \right) \right] \end{aligned} \quad (61)$$

so that

$$\Gamma \propto \exp \left[- \left(\frac{r}{\hat{r}_r} \right)^{(3-g)/3} \right] \quad (62)$$

where r_1 and ρ_1 are some fiducial radius and the corresponding density, and where $\hat{r}_r = (r_r(\rho_1)^3 r_1^{-g})^{1/(3-g)}$.

4.1.5. Observational concerns

Throughout this discussion, we have tacitly assumed that the spherical fireball does fit the GRB 970508 observations well, so that difficulties with the various beaming models offer support to the spherical model. This is open to question. In defense of the spherical model, Reichart (1997) has studied the largest available afterglow data set from a single optical observatory (that of Sokolov et al 1997) and finds that the afterglow of GRB 970508 is well fitted using a standard model with the addition of a modest amount of dust extinction at high redshift. By using a single data set, he minimizes many of the possible systematic errors, such as inconsistent zero points for absolute photometry.

On the other hand, if one examines the spectral slope from mixed data sets over larger wavelength intervals (optical - near infrared) and a larger time range, we find some worrying data points. In particular, the HST observations (Pian et al 1998) exhibit a spectral slope $\alpha \approx 1.5 \pm 0.3$ based on quoted R ($0.7\mu\text{m}$) and H ($1.6\mu\text{m}$) band magnitudes from the STIS and NICMOS instruments. The

observed slope in Sokolov et al's data is 1.1, which Reichart interprets as a reddened spectrum with intrinsic slope 0.8. The HST data point is thus in mild conflict with the Sokolov et al observation. The significance of this conflict is unclear, since the error on the HST data is dominated by calibration uncertainties.

Likewise, if we compare the spectral slopes inferred from the Keck K_s band data (Morris et al 1997) and near contemporaneous optical data (Djorgovski et al 1997; Keleman 1997), we find slopes of 0.24 ± 0.12 at $t_{\oplus} = 4.35$ day and 0.40 ± 0.10 at $t_{\oplus} = 7.35$ day. These are now substantially bluer than the value from Sokolov et al. The first of these may simply indicate that the K band flux has not yet passed its peak and entered the power law decay phase; scaling from the R band peak at $t_{\oplus} \approx 1.9$ day gives a K band peak at ~ 4.1 day. The second is harder to explain physically but easier observationally, because the R band flux estimate is based on an unfiltered observation that may have (for example) a substantial color term.

The net effect of such outlying data points is illustrated by the light curve fits in Rhoads 1999b. These fits achieve χ^2 per degree of freedom around 3.6 in fitting to a large compilation of R band data (Garcia et al 1998). It is not likely that any current model can do better without discarding either predictive power or outlying data points.

In summary, the spherical model does fit the GRB 970508 afterglow model better than the beamed model developed in this paper for any beaming angle $\zeta_m < 0.5$ radian. There are a few discrepancies in the measured spectral slopes. If these are real, they pose a challenge to standard fireball models. However, they could merely be indicative of calibration problems in inhomogeneous data. It is noteworthy that Sokolov et al (1997), who have the largest multiband data set from a single telescope, find no evidence for spectral slope evolution over the interval $2 \text{ day} \leq t_{\oplus} \leq 5 \text{ day}$.

5. CONCLUSIONS

We have shown that under a simple model of beamed gamma-ray bursts, the dynamical evolution of the burst remnant changes at late times. This change introduces a break in the light curve, which is potentially observable. The afterglows of GRB 970508, 970228, and 971214 showed no convincing evidence for such breaks, and their combined spectral slopes and light curves are inconsistent with the predictions of this beamed model. This implies that beaming tests based on blind searches for afterglows must be prepared to identify transients whose properties differ appreciably from the properties of these approximately spherical afterglows. Some more recent afterglows (GRB 990123; GRB 980519) better match beamed burst models, and may provide more suitable templates for these searches.

Comparing our model with late time optical and radio observations, we suggest that GRB 970508 was effectively unbeamed. This implies energy requirements that are near the canonical isotropic values for cosmological distances, and are not greatly mitigated by strong beaming. No straightforward variation on our beamed fireball model seems likely to simultaneously explain the observed spectral slope and a pure power law light curve decaying at the

observed rate. We conjecture that strongly beamed fireball models cannot explain all observed gamma ray burst afterglows without substantially altering at least one major ingredient of the models. We therefore obtain the first lower bound on GRB energy requirements that does not involve assumptions about beaming: $E \gtrsim 3 \times 10^{49}$ erg. This limit will increase by an order of magnitude if the same material that gives rise to the optical afterglow causes either the X-ray afterglow or the gamma ray emission, and will rise further if the burst's energy is not converted to radiation with perfect efficiency.

I wish to thank Ralph Wijers, Jonathan Katz, Tsvi Piran, Eli Waxman, Daniel Reichart, Alexander Kopylov, David De Young, and Sangeeta Malhotra for helpful communications. I also wish to thank Infrared Processing and Analysis Center for hospitality during the course of this work. Finally, I wish to thank all those who worked to achieve accurate gamma ray burst position measurements and so opened the way for afterglow studies. This work was supported by a Kitt Peak Postdoctoral Fellowship. Kitt Peak National Observatory is part of the National Optical Astronomy Observatories, operated by the Association of Universities for Research in Astronomy.

REFERENCES

- Bond, H. E. 1997, IAU Circular 6654
- Castro-Tirado, A. J., Gorosabel, J., Greiner, J., Zapatero-Osorio, M. R., & Costa, E. 1997, IAU Circular 6800
- Castro-Tirado, A. J., et al 1999, to appear in *Science*, 26 March 1999
- Costa, E. et al 1997, IAU Circular 6572
- Dar, A. 1997, preprint (astro-ph/9709231)
- Djorgovski, S. G., Metzger, M. R., Kulkarni, S. R., Odewahn, S. C., Gal, R. R., and Pahre, M. A., Frail, D. A., Costa, E., and Feroci, M. 1997, IAU Circular 6660
- Djorgovski, S. G., Kulkarni, S. R., Ramaprakash, A. N., & Frail, D., on behalf of the Caltech GRB collaboration, 1998, GCN notice 025
- Frail, D. A., Kulkarni, S. R., Nicastro, L., Feroci, M., & Taylor, G. B. 1997, *Nature*, 389, 261
- Garcia, M. R. et al 1998, *ApJ* 500, L105
- Goodman, J. 1986, *ApJ* 308, L47
- Goodman, J. 1997, *New Astronomy*, 2, 449
- Groot, P. et al 1997, *ApJ*, 493, L27
- Katz, J. I. 1994, *ApJ* 422, 248
- Katz, J. I., & Piran, T. 1997a, *ApJ* 490, 772
- Katz, J. I., & Piran, T. 1997b, presentation at 4th Huntsville GRB Symposium, astro-ph/9712242
- Keleman, J. 1997, *International Bulletin of Variable Stars* 4496.
- Kouveliotou, C., Briggs, M. S., Preece, R., Fishman, G. J., Meegan, C. A., & Harmon, B. A., on behalf of the CGRO BATSE team, 1997, IAU Circular 6660
- Kulkarni, S. R., et al 1999, *Nature*, in press, astro-ph/9902272
- Meegan, C. A., Pendleton, G. N., Briggs, M. S., Kouveliotou, C., Koshut, T. M., Lestrade, J. P., Paciesas, W. S., McCollough, M. L., Brainerd, J. J., Horack, J. M., Hakkila, J., Henze, W., Preece, R. D., Mallozi, R. S., & Fishman, G. J. 1996, *ApJS* 106, 65
- Morris, M., Mastrodemos, N., Zuckerman, B., McCarthy, C., Becklin, E., Lowrance, P., Chary, R., and Barnbaum, C. IAU Circular 6666
- Mészáros, P., & Rees, M. J. 1997a, *ApJ* 476, 232
- Mészáros, P., & Rees, M. J. 1997b, *ApJ* 482, L29
- Mészáros, P., Rees, M. J., & Wijers, R. A. M. J. 1997, astro-ph/9709273
- Metzger, M. R., Djorgovski, S. G., Kulkarni, S. R., Steidel, C. C., Adelberger, K. L., Frail, D. A., Costa, E., & Frontera, F. 1997, *Nature*, 387, 879
- Pacholczyk, A. G. 1970, *Radio Astrophysics*, San Francisco: W. H. Freeman
- Panaitescu, A., Mészáros, P., & Rees, M. J. 1998, preprint (astro-ph/9801258)
- Panaitescu, A., & Mészáros, P., 1999, submitted to *ApJ*
- Paczyński, B. 1986, *ApJ* 308, L43
- Paczyński, B., & Rhoads, J. E. 1993, *ApJ* 418, L5
- Paczyński, B. 1997, preprint (astro-ph/9706232)
- Paczyński, B. 1998, *ApJ* 494, L45
- Pedersen, H., et al 1998, *ApJ* 496, ??? (astro-ph/9710322)
- Pian, E., Fruchter, A. S., Bergeron, L. E., Thorsett, S. E., Frontera, F., Tavani, M., Costa, E., Feroci, M., Halpern, J., Lucas, R. A., Nicastro, L., Palazzi, E., Piro, L., Sparks, W., Castro-Tirado, A. J., Gull, T., Hurley, K., & Pedersen, H. 1998, *ApJ* 492, L103
- Rees, M. J., & Mészáros, P. 1998, *ApJ*, submitted (astro-ph/9712252)
- Reichart, D. E. 1997, preprint (astro-ph/9712100)
- Reichart, D. E. 1998, preprint (astro-ph/9801139)
- Rhoads, J. E. 1997a, *ApJ* 487, L1
- Rhoads, J. E. 1997b, presentation at 4th Huntsville GRB Symposium (astro-ph/9712042)
- Rhoads, J. E. 1999b, to appear in A&AS (proceedings of the Rome workshop on "Gamma Ray Bursts in the Afterglow Era"), astro-ph/9903400 (?)
- Rybicki, G. B., & Lightman, A. P. 1979, *Radiative Processes in Astrophysics*, New York: John Wiley & Sons
- Sari, R. 1997, *ApJ* 489, L37
- Sari, R., Piran, T., & Narayan, R. 1998, *ApJ* 497, L17
- Sari, R., Piran, T., & Halpern, J. P. 1999, astro-ph/99033
- Sokolov, V. V., Kopylov, A. I., Zharikov, S. V., Costa, E., Feroci, M., Nicastro, L., & Palazzi, E. 1997, presentation at 4th Huntsville GRB Symposium (astro-ph/9709093)
- Van Paradijs, J., et al 1997, *Nature* 386, 686
- Vietri, M. 1997a, *ApJ* 478, L9.
- Vietri, M. 1997b, astro-ph/9706060
- Waxman, E. 1997a, *ApJ* 485, L5
- Waxman, E. 1997b, *ApJ* 489, L33
- Waxman, E., Kulkarni, S. R., & Frail, D. A. 1998, *ApJ* 497, 288
- Weedman, D. W. 1986, *Quasar Astronomy*, Cambridge: Cambridge University Press
- Woods, E., & Loeb, A. 1995, *ApJ* 453, 583
- Wijers, R. A. M. J., Rees, M. J., & Mészáros, P. 1997, *MNRAS* 288, L51
- Wijers, R. A. M. J., & Galama, T. J. 1998, astro-ph/9805341

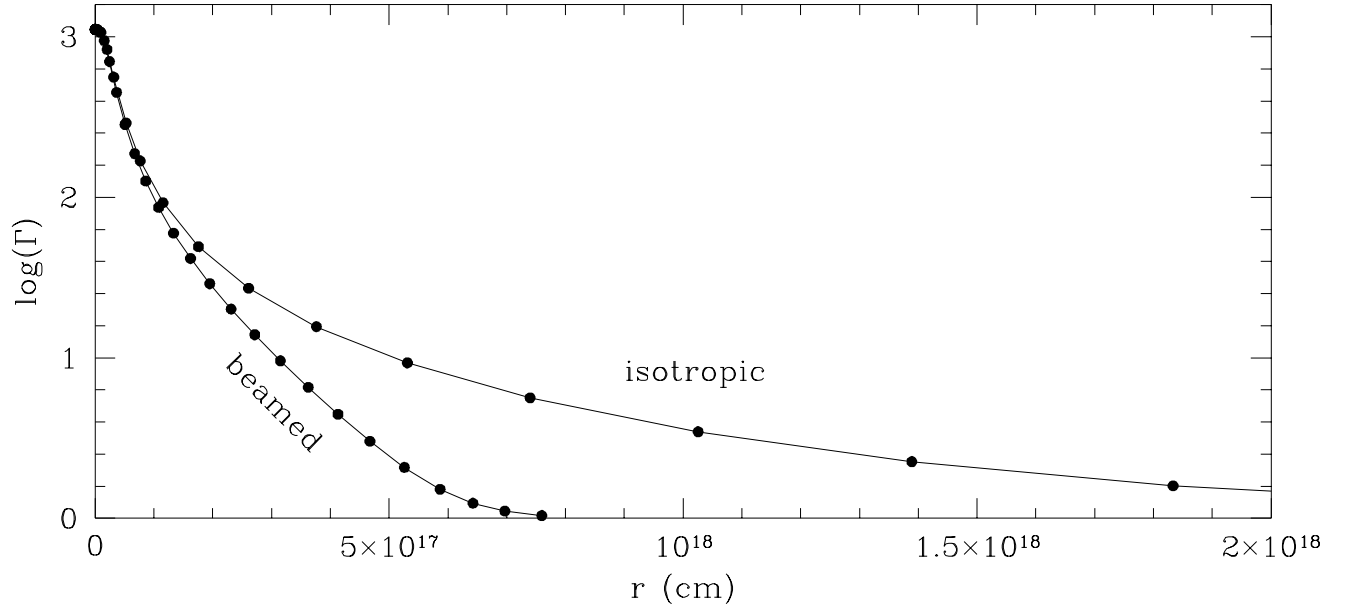


Fig. 1.— Dependence of the bulk Lorentz factor Γ on the burst expansion radius for an isotropic burst and a burst beamed into an opening angle $\zeta_m = 0.01$ radian. Both bursts follow a $\Gamma \propto r^{-3/2}$ evolution initially, but the beamed burst changes its behavior at $\Gamma \approx 100 \approx 1/\zeta_m$, beyond which its Lorentz factor decays exponentially with radius.

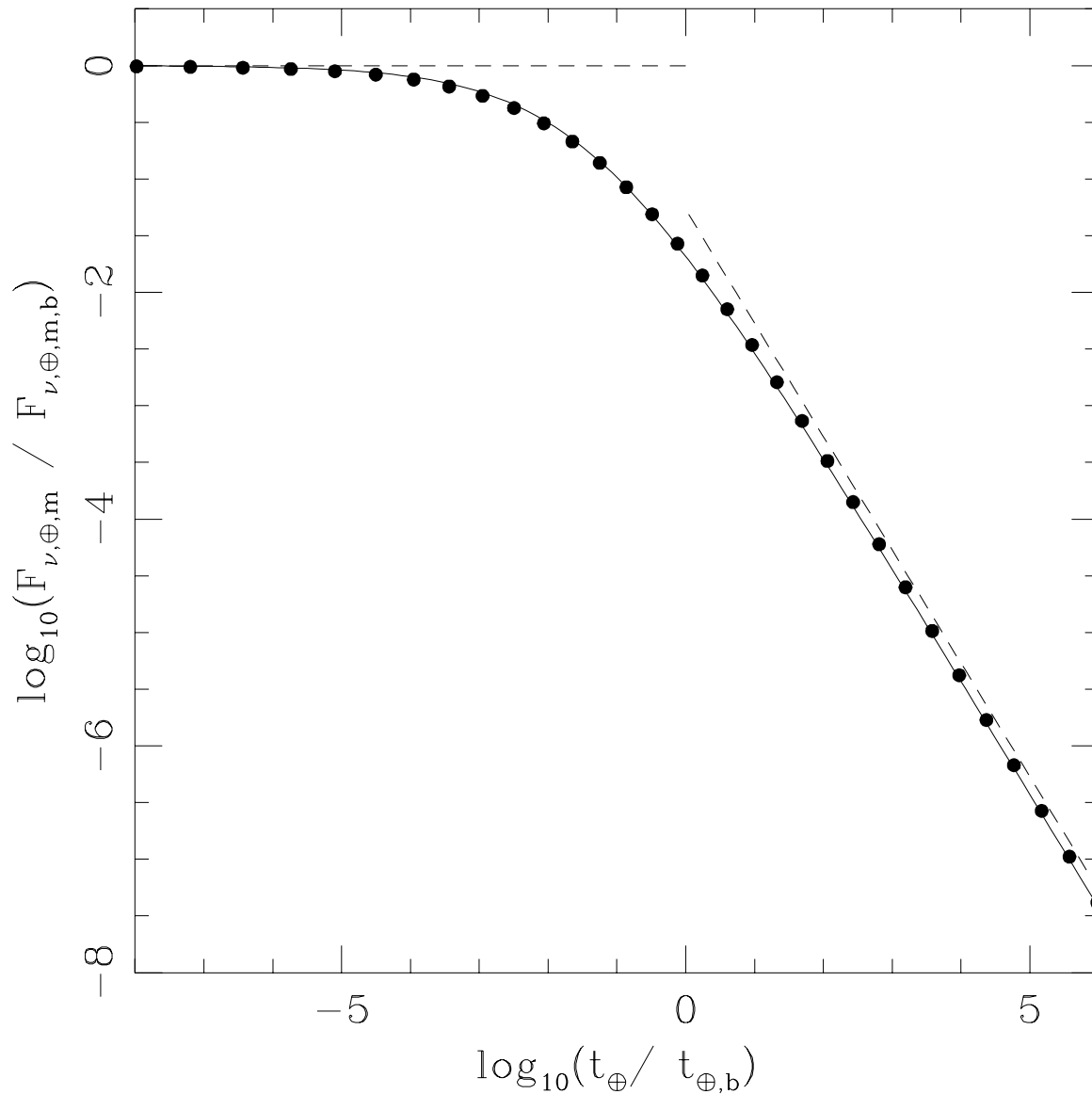


Fig. 2.— Dimensionless peak flux as a function of dimensionless observer-frame time. Points show the results of numerical integrations. Dashed lines show the analytic asymptotic forms from equations 30 and 40, scaled to fiducial values as described in section 3.2.4. The late-time flux density is below the prediction of equation 40 by a factor of ~ 0.7 . This stems from approximations in the exponential regime initial conditions (equations 16 to 19), which are derived by applying the power law regime results beyond their range of strict validity. The solid curve shows an empirical interpolation between the early and late-time analytic forms, incorporating a factor 0.7 correction to the late-time asymptotic form (see section 3.2.5).

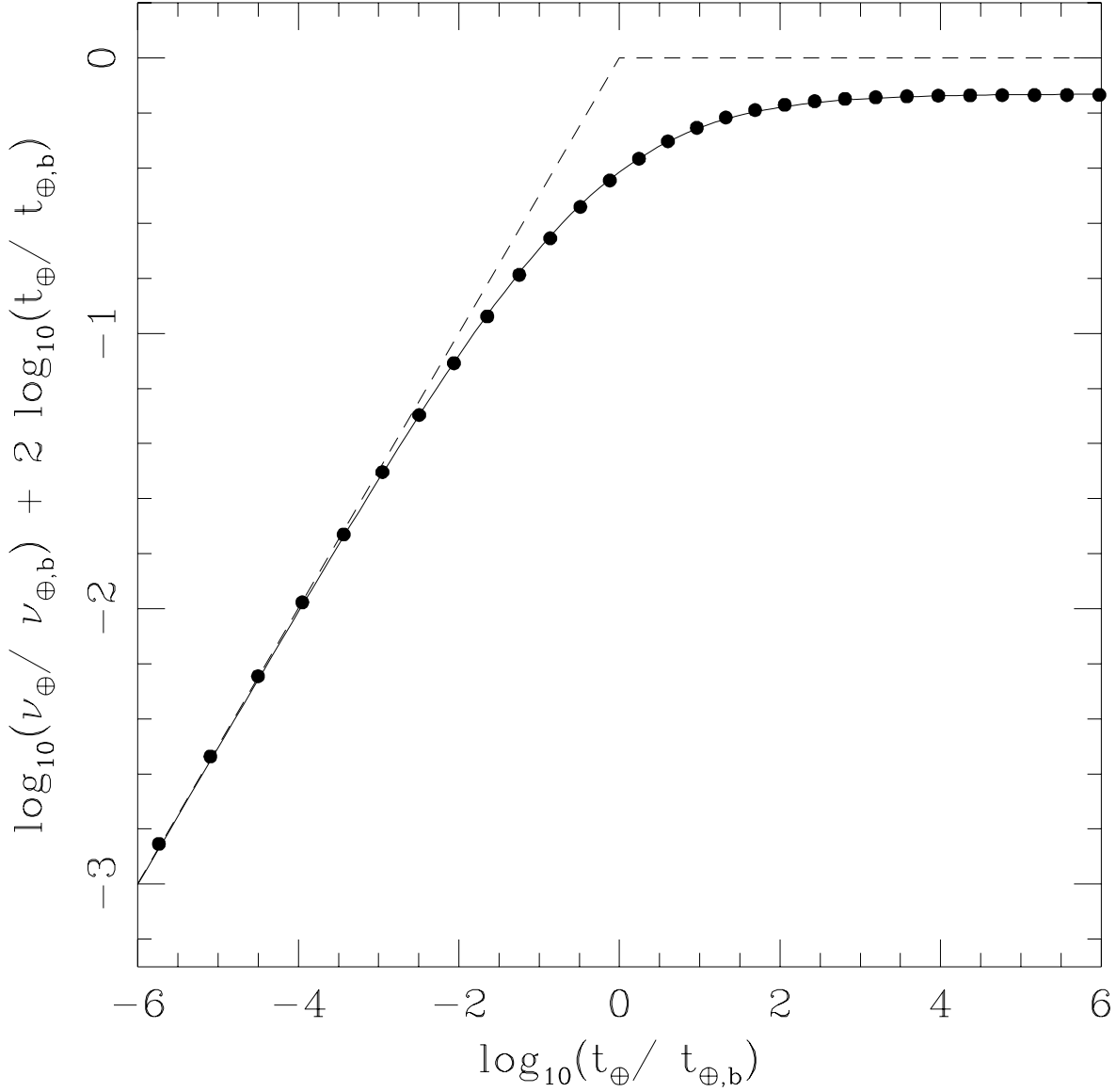


Fig. 3.— Dimensionless frequency at which the spectrum peaks as a function of dimensionless observer-frame time. The y -axis shows $\log_{10}(\nu_{\oplus,m} t_{\oplus}^2)$, so that a t_{\oplus}^{-2} decay of peak flux density with time appears as a horizontal line. As in figure 2, points show the results of numerical integrations; dashed lines show analytic asymptotic forms (here from equations 28 and 34), and the solid line is an empirical interpolation. The late-time asymptotic frequency given by equations 34 is seen to be too large by a factor ~ 1.35 . This is due to the approximate initial conditions used to derive equation 34, and a correction factor has been applied in deriving the interpolated curve (see section 3.2.5).

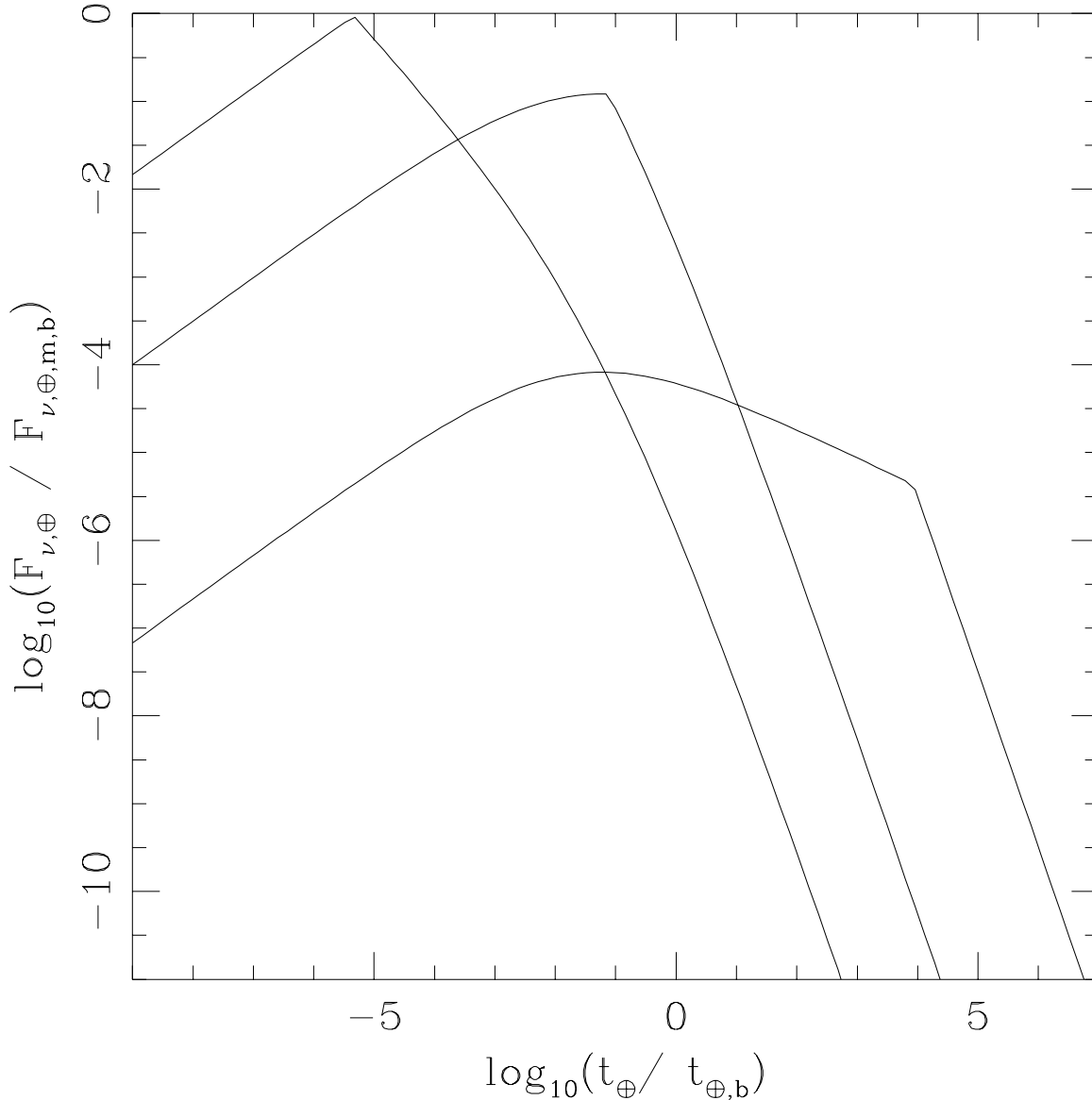


Fig. 4.— Sample light curves in dimensionless units. The curves have been derived by combining a broken power law spectrum (with electron energy distribution slope $p = 2$) with the interpolated, dimensionless forms of the $F_{\nu,m,\oplus}(t_{\oplus})$ and $\nu_{\oplus,m}(t_{\oplus})$ relations (see section 3.2.5 for details). The light curves correspond to frequencies $10^8\nu_{\oplus,m,b}$, $10^{1.5}\nu_{\oplus,m,b}$, and $10^{-8}\nu_{\oplus,m,b}$, in order of decreasing flux density at the earliest time plotted. All the asymptotic behaviors described in equations 50 are exhibited here, though the additional cooling break (equation 51) is omitted. The transition between the behaviors for $t_{\oplus} \ll t_{\oplus,b}$ and $t_{\oplus} \gg t_{\oplus,b}$ is rather gradual. The other transition, between $t_{\oplus} \ll t_{\oplus,m}(\nu_{\oplus})$ and $t_{\oplus} \gg t_{\oplus,m}(\nu_{\oplus})$, is artificially sharp in these plots because the adopted spectrum has a discontinuous slope at $\nu_{\oplus,m}$. A more detailed treatment of the spectrum would smooth out this transition also.